FLUCTUATING LIFT ON CYLINDERS OF RECTANGULAR CROSS SECTION IN SMOOTH AND TURBULENT FLOWS

by

FARSHID NAMIRANIAN

B.S., UNIVERSITY OF WASHINGTON, U.S.A., 1982

A THESIS SUBMITTED IN PARTIAL FULFILMENT OF

THE REQUIREMENTS FOR THE DEGREE OF

MASTER OF APPLIED SCIENCE

in

FACULTY OF GRADUATE STUDIES

DEPARTMENT OF MECHANICAL ENGINEERING

We accept this thesis as conforming

to the required standard

UNIVERSITY OF BRITISH COLUMBIA

APRIL, 1985

In presenting this thesis in partial fulfilment of the requirements for an advanced degree at the UNIVERSITY OF BRITISH COLUMBIA, I agree that the Library shall make it freely available for reference and study. I further agree that permission for extensive copying of this thesis for scholarly purposes may be granted by the Head of my Department or by his or her representatives. It is understood that copying or publication of this thesis for financial gain shall not be allowed without my written permission.

DEPARTMENT OF MECHANICAL ENGINEERING

UNIVERSITY OF BRITISH COLUMBIA
2075 Wesbrook Place
Vancouver, Canada
V6T 1W5

Date: APRIL, 1985

ABSTRACT

This thesis presents an experimental investigation of the fluctuating lift (or side force) coefficient on fixed two dimensional rectangular cylinders for various free stream turbulence intensities and scales. The measurements are made using turbulence producing devices such as grids and circular rods placed upstream of the stagnation line of the model. Measurements are reported for three fixed rectangular prisms with B/H of .5, .67 and 1 where H is the frontal dimension and B is the streamwise width of the body.

The method of measurement made it possible to vary the body span so that the correlation of the fluctuating side force over the body span could be investigated. It was shown that for low turbulence intensity, the spanwise correlation of the fluctuating side force over the square cylinders decreases by a large amount with increasing span. For higher turbulence intensity this decrease was reduced, and for $u'/U \simeq 10\%$ there was essentially no decrease of fluctuating lift coefficient with increase of span.

Table of Contents

LIST OF TABLES

LIST OF FIGURES

NOMENCLATURE

b :bar width of a grid

B :streamwise dimension of rectangular sections

C :damping

C_D :drag coefficient

C_L' :r.m.s. lift coefficient

C_{L_0}' :local value of C_L', measured over a very short span without end effects

d :rod diameter

dB :decibel

f_n :natural frequency (Hertz)

f_v :vortex shedding frequency (Hertz)

F :magnitude of the force applied to the 'live' section

F_0 :local force on a live section

F_1 :local force on a live section

F_2 :local force on a live section

F_B :total force on the live section

H :frontal dimension of rectangular sections

$H(\omega)$:mechanical admittance

Hz :Hertz, cycles/sec.

k :stiffness

L :span of the live section

L' :effective length ($L-2\Delta$)

L_x :longitudinal length scale of turbulence

m :mass

M :mesh width of a grid

Re :Reynolds number = $U H/\nu$

t :time

T :integral time scale

u' :longitudinal component of fluctuating speed

U :wind speed (mean)

u'/U :turbulence intensity

x :deflection of the beam (amplitude of motion)

$\sqrt{\overline{x^2}}$:r.m.s deflection

Y :spanwise distance from the mid span of a rectangular cylinder

ω_v :vortex shedding frequency (radians/sec)

ω_n :natural frequency (radians/sec)

ρ :air density

ν :kinematic viscosity

β :damping as a fraction of critical (i.e. β=C/Cc)

Δ :length, affected by end condition

τ :time delay

λ :integral length scale of the force correlation

ACKNOWLEDGEMENTS

The author considers himself fortunate to have had Dr. I.S.Gartshore as his supervisor throughout this study.

Thanks to the department of Mechanical Engineering for the use of their facilities, and to the technical staff for its effort in constructing the wind tunnel models and mountings.

Finally, the author would like to express his sincere thanks to those who contributed in this study in any way.

1. INTRODUCTION

Forces induced by vortex shedding on circular cylinders have been measured by numerous researchers. However, the phenomenon of fluctuating side forces (fluctuating lift) on rectangular cylinders in smooth and turbulent flows has received less attention. The fluctuating side force is due to alternate shedding of vortices from the sides of the cylinders; the variation of local pressure distribution due to shedding of the vortices causes a time varying force on the cylinder, at a frequency centered around the vortex shedding frequency.

The subject is of importance because of the effects of wind induced vibrations which cause material fatigue and resonant vibrations of structures (resonant vibrations occur when the frequency at which the eddies are shedding away from a cylinder, i.e., vortex shedding frequency, matches the natural frequency of the cylinder). Resonant vibrations of slender towers, chimney stacks and transmission lines are possible examples.

This work deals only with the fluctuating lift due to vortex shedding. Particularly when turbulence is present in the free stream, buffeting forces arise which are spread over a wide range of frequencies. These are significant for bodies of rectangular section on which flow separation followed by permanent reattachment occures, typically bodies whose streamwise length is larger than their frontal dimension. Such buffeting forces are not expected to be

significant in the present studies since only relatively short sections are used.

The distinction must be made here between local lift and lift averaged over a finite span. The lift per unit length averaged over a finite span includes the imperfect spanwise correlation of the force, and is always less than the lift per unit length measured locally if end effects do not enter. Local forces are found either by directly measuring the force on very short spans or by measuring a series of pressures (either simultaneously or with suitable phase correlation) to deduce the local force. The use of pressure measurements is most common since very short span lengths sense only very low forces which are difficult to measure directly. Forces on longer span 'live' sections can be measured directly or deduced from local forces and the spanwise correlation of force. The former has the difficulty that the 'live' section must be physically separated from adjacent 'dummy' end sections. Even very narrow gaps (as in Vickery's[1] case) may give rise to unwanted fluctuating pressures or spanwise pressure gradients and hence unwanted forces on the 'live' section. Thus end effects enter in a variable way, proportionally larger effects being present for shorter spans.

The direct measurement of spanwise force correlation is difficult because of the need for many pressure taps or complicated force sensor arrangements, and is usually replaced by a spanwise correlation of pressures measured at

mid chord and assumed to be equivalent to the correlation of forces. This equivalence is somewhat doubtful although it is best when measured as a correlation of pressure difference on either side of the model as was done by Vickery[1].

A review of prominent papers in this field shows that the measurement of local fluctuating forces is fairly common. Of these, Pocha[2], Lee[3], Wilkinson[4], Gartshore[5] and Bearman & Obasaju[6], measured forces on square 2D cylinders all using integration of pressures. Fewer writers have used finite span 'live' sections to measure spanwise averaged forces. Vickery[1] measured the fluctuating side forces on a 6in(15.24cm) by 6in(15.24cm) square cylinder of 3in(7.62cm) length. The model was mounted on a hollow beam with four elastic supports and, using a uni-directional strain gauge dynamometer mounted within the beam, the fluctuating side forces could be measured. The gap between the 'live' section and the dummy ends was set at .01in(.25mm).

In a similar study, now considering a circular cylinder, So & Savkar [7] measured the spanwise correlation of the fluctuating side forces and drag on circular cylinders, in smooth and turbulent flows for different Reynolds numbers, using two three-axis measuring load cells at each end of their test cylinder. In these tests, the 'live' span could vary from 1.5in (38.1mm)to 8in(203.2mm), and a rubber seal was used at the ends of the 'live' section.

In this type of experiment, the natural frequency of the model is usually made as high as possible by using a

light 'live' section, stiffly mounted. At most wind speeds, the vortex shedding frequency f_v, where $f_v = SU/H$ (with Strouhal number S and frontal dimension H), is then well below the model natural frequency f_n. As wind speed is increased however, f_v approaches f_n and large resonant vibrations occur. These large motions are undesirable, for reasons which will appear later, and wind speeds are usually restricted to values for which $f_v/f_n \leq 1/4$. In Vickery's case, for example, the natural frequency of the model was about 180HZ and Vickery took meaurements for vortex shedding frequencies below 50 cycles/sec.

Typical results from all these papers are summarized in Table 1.

In this thesis, measurements on 'live' lengths of various spans are used to deduce the forces to which the section is subjected. This is considered most realistic because actual structures having similar end effects are subject to forces equivalent to those actually measured here, so that the present data is most likely to be useful in design. The work to be described here investigates the spanwise averaged fluctuating side forces on sharp edged rectangular prisms of various spans and shapes, in smooth and turbulent flows. The experimental method used is similar to that used by Vickery[1] and So & Savkar[7].

It has been suggested that the fluctuating side force varies with free stream turbulence in a similar way to that of the base pressure (see e.g. Gartshore[5]) . The

experimental study reported here explores the possibility. It also shows the effect of free stream turbulence and aspect ratio (span/frontal dimension) on the vortex induced fluctuating side force exerted on rectangular sections.

2. EXPERIMENTAL ARRANGEMENTS

2.1 WIND TUNNEL

The experiments were conducted in the U.B.C. low speed, low turbulence, closed return type wind tunnel in which the velocity can be varied between 0 and 46m/s with a turbulence level of less than .1%.

Three screens smooth the flow at the entrance of the settling chamber and a 7:1 contraction accelerates it, improving its uniformity as it reaches the test section. The test section is 2.74m long with a cross section of 91.4 by 68.6cm. Four 45 degrees fillets, decreasing from 15cm at the upstream to 12cm at the downstream end, offset the effect of boundary layer growth in the test section.

The tunnel is powered by a 15HP direct current motor, driving a commercial axial flow fan with a Thyrister system of speed control. The pressure drop across the contraction is measured on a Betz micro-manometer with a precision of .02 mm of water. The air speed in the test section is calibrated against the pressure drop. Fig 1 shows the outline of the tunnel.

2.2 TURBULENCE PRODUCING DEVICES

2.2.1 GRIDS

In the experiment four square mesh grids were used for producing different levels of turbulence

intensity and different turbulence scales. Three of the grids were of rectangular bars with mesh widths of 9in(228.6mm), 4.5in(114.3mm) & 2in(50.8mm) and bar widths of 2.25in(57.15mm), 1.1in(27.94mm) & 0.5in(12.7mm) respectively. The fourth grid (the smallest mesh width grid) had round bars with a mesh width of 0.256in(6.5mm) and bar diameter of 0.0381(.97mm). Grids were mounted at the upstream end of the test section, in every case.

The quality of the resultant flow at some distance downstream of the grid, has been shown to be nearly isotropic homogeneous turbulence superimposed on a uniform mean flow (see for example Bains and Peterson [8]). Therefore, grid turbulence appears to be the simplest form of turbulence for two dimensional tests, having a flat velocity profile and a uniform turbulence intensity distribution.

Bains and Peterson[8] found that if the flow is to be nearly uniform, the model can be no closer than 5 to 10 mesh widths from the grid. Thus the model position was chosen to be 72in(183cm) (8 times the largest mesh width) away from the grids to have a reasonably uniform flow at the model face for all cases.

The characteristics of the turbulence acheieved by the grids were measured by a single hot wire with

linearized response, traversed longitudinally in the mid span of the tunnel. The wire was of tungsten with a diameter of 5 microns. The hot wire system used was a Disa type 55D01 with suitable linearizer. A low pass filter of the type Disa 55D25 was set to remove any frequency higher than 10KHZ. Using suitable voltmeters the relative turbulence intensity u'/U was deduced. A typical calibration curve of the hot wire is shown in Appendix A. For each grid in position inside the tunnel, the hot wire was used to calibrate the Betz manometer readings against the tunnel speed, so that the Betz manometer could be used later as a measure of mean wind speed.

The autocorrelation of the linearized velocity was measured using a P.A.R. 101 correlator. The integral time scale was found by integrating the auto correlation function over various time delays. Appendix A shows a typical auto correlation curve and describes the method of obtaining the integral time scale. Using Taylor's Hypothesis, the integral length scale $L_x = U \cdot \tau$ was deduced. Figure 2 shows the decay of the longitudinal component of intensity for the four grids. Data for a uniplanar grid obtained by Vickery[9] agree very well, while the results obtained by Campbell and Etkin[10], and Surry[11] depart from the present data slightly.

Data for a similar grid from Baines and Peterson[8] are somewhat lower. Also, the curve $u'/U=1.12(x/b)^{-5/7}$ which is a best fit to Bains' and Peterson's data for different grids is lower than the present values. Data from McLaren et al.[12] and Laneville[13] agree very well. Fig. 3 shows the growth of the longitudinal scale of turbulence with downstream distance. The result agrees fairly well with those of Vickery[9] and Laneville[13]. The two lines show the scatter limit for corresponding data by Van der Hegge Zignen [14].

2.2.2 RODS

As an alternate to the use of grids, a 0.5in(12.7mm) diameter rod was traversed along the tunnel, upstream of the square prism centre line, to produce different levels of upstream turbulence. The rod was placed between 20d and 70d from the front face of the model where d is the rod diameter. This produced intensities between 12% and 4% on the rod wake centre line at the model location. Turbulent intensities were found from the measurements of Gartshore[15], and integral longitudinal length scales, again on the rod centre line, from the measurements of Townsend[16].

2.3 MODELS AND MOUNTINGS

For each of the three rectangular sections of B/H=1, .67 and .5, five models were made with lengths L of; 1.5in(38.1mm), 3in(72.6mm), 6in(152.4mm), 12in(304.8mm) and 24in(609.6mm). Each model had a frontal dimension H of 1.5in(38.1mm), so that blockage ratios were always 4.2% based on frontal area (see fig. 4 for model details). There was no blockage correction applied to the data since there is no secure correction technique for fluctuating quantities available. In this kind of test, the trend is more important than any absolute value in any case.

A 29in(736.6mm) aluminum beam with 1/4in(6.35mm) by 1/2in(12.7mm) cross section, having two strain gauges at each end, was used as a uni-directional load cell. This could sense the cross stream loads on the 'live' measuring section attached to it (see fig. 5). Two 2in(50.8mm) by 2in(50.8mm) holes were made in the roof and floor of the tunnel on a vertical line perpendicular to the axis of symmetry of the tunnel at the desired position. A heavy steel frame, surrounding the tunnel test section was used to hold the beam in position. The frame stood on four adjustable legs without touching the tunnel, so that vibrations of the tunnel would not affect the frame. The load cell beam passed through the holes in the tunnel walls and was fastened to the frame at each end, by means of specially made clamps. Fig. 6 gives more details of the mounting. Dummy end pieces were screwed to the tunnel walls

and end plates were mounted on them. The distance from the end plates to the floor and roof of the tunnel was 1.5in(38.1mm), so that they were outside the tunnel wall boundary layers.

Stansby[17] showed that end effects altered the true base pressure over the whole length of a 2D circular cylinder without end plates. He showed that end plates improved the base pressure to its "true" value.

Obasaju[18] concluded that for sharp edged 2D square cylinders, end plates were again of importance.

In this work, one set of end plates was used for all models as shown in fig. 7.

For each experiment the 'live' model's span was screwed to the centre of the load cell beam and the proper dummy end pieces were fastened to the tunnel roof and floor. The gap between the 'live' section and adjacent dummy end sections was always made less than .02in(.5mm).

2.4 FORCE MEASUREMENTS

The average fluctuating side forces caused by vortex shedding from a two dimensional bluff body at zero incidence can be measured over a finite span by the methods used by Vickery[1] and So & Savkar[7]. The average fluctuating side force is altered by having different end conditions for the 'live' section. In the work to be described here two end conditions were considered: a simple gap less then .02in(.5mm) between the 'live' section and dummy end pieces;

and the same gap but with a set of end plate identical to those in fig. 7, attached to the ends of the 'live' section.

Each time a model was mounted on the load cell beam, a calibration of the load cell was done as load versus strain gauge voltage output. The calibration of load versus deflection was also measured periodically. The natural frequency and the damping of each model was different because of different sizes and weights of the models. Using a spectrascope the natural frequency of the models was measured prior to the test. Their damping was always less than 1% as a fraction of critical, as measured on an oscilloscope. Each model was tested at wind speeds of 2m/s and higher. The fluctuating signal from the strain gauge bridge amplifier was fed into a fixed 1 to 100 signal-amplifier and then through a low pass filter to cut off frequencies near f_n, the model natural frequency. Using a true r.m.s. voltmeter, the r.m.s. of the fluctuating signal was read, and from the calibration, the r.m.s. deflection of the beam was found. Using a spectrascope the average vortex shedding frequency at each wind speed was found.

For one degree of freedom, the equation of motion of the load cell beam is:

$$m\ddot{x}+c\dot{x}+kx=F(t)=F_1\mathrm{Sin}(\omega_1 t)+F_2\mathrm{Sin}(\omega_2 t)+\ldots$$

Assuming the vortex shedding occurs in a narrow range

centered about f_v, this can be solved for a range of frequencies to give:

$$C_L' = \frac{\sqrt{\overline{x^2}}/B}{H(f_v)} \quad \frac{k}{1/2\rho U^2 L}$$

where $\sqrt{\overline{x^2}}$ is the r.m.s. of deflection, B the streamwise dimension of the prism, L length of the 'live' section, k the stiffness of the load cell beam and $H(f_v)$ mechanical admittance evaluated at the vortex shedding frequency (see appendix B for more details of the derivation). Using this equation and the data obtained from the experiment, C_L' at each wind speed was found. This method assumes that the force oscillates near a single frequency; the range of vortex frequencies was not measured in this experiment, but was limited to values less than 20Hz below f_n.

To make the assumption that the cylinders are 'rigid' , the motion of the live section must be very small compared to the section size. The r.m.s. amplitude of the 'live' section was measured, and was found to be less than .1% of H in all cases. Although it is known that cylinders are sensitive to small motions, this small motion is assumed here to be negligible, and the cylinders are described as rigid.

2.5 PRESSURE MEASUREMENTS

Mean base pressure measurements were made on a fixed 1.5in(38.1mm) by 1.5in(38.1mm) square cylinder spanning the tunnel vertically. The base pressure was measured to see the effect of different end conditions and also to compare with the results of Lee[19] and Obasaju[18]. The square prism was prepared with twenty pressure taps on the rear face at the mid chord, spread over most of the total span. The base pressure was measured in smooth and turbulent flows, with and without end plates mounted on the model. End plates were 1.5in(38.1mm) away from the walls of the tunnel as before. The base pressures measured in this test are shown in figure 8 and are quite comparable to Obasaju's results.

3. RESULTS AND DISCUSSION FOR SQUARE SECTIONS

3.1 FORM OF RESULTS

In sharp edged bluff bodies like rectangular prisms the point of separation of the flow is fixed and C_D, drag coefficient, does not vary for high enough Re. All force coefficients should therefore be independent of Reynolds number or of wind speed, provided transition to turbulence occurs rapidly in the separation shear layers. This appears to be the case for Re$\geq 10^4$ (see e.g. Gartshore[15]). The range of Re in this experiment was $0.5 * 10^4$ to $2.2 * 10^4$ based on frontal dimension. If the flow pattern is independent of Re, as is expected, and if no end effects or difficulties of measurement occur, the deduced values of C_L' should be the same at all speeds. Measured results of fluctuating lift coefficient versus wind speed, for one case, are plotted in fig. 9. Another effect which was observed in some cases, was resonant motion of the load cell beam at a speed where f_v is a lower harmonic of f_n (see e.g. fig. 10). Measurements at this wind speed were avoided since this effect caused an undesirable motion of the beam and an increased r.m.s. force reading. It was not always posssible to remove this effect by using a low pass filter. At high speeds, when the vortex shedding frequency was close to the natural frequency, the amplitude of the natural frequency vibrations increased. Again the r.m.s. voltage readings were incorrect, being higher than the value appropriate for vortex shedding forces

only. This problem was solved at low speeds by using a low pass filter to cut out the effect of natural frequency vibrations, but for high speeds the low pass filter also cut out some of the desirable signals from the vortex shedding. The data was corrected for the effect of filter and amplifier used. A calibration curve for the filter is shown in appendix A.

Choosing an average of the most desirable data points, the C_L' for each model was found (see fig. 9).

When the rod was used as a turbulence producing device, C_L' was measured at just one speed (4m/s) for each 'live' section at every rod position.

C_L' values obtained for square sections with end plates (see figs. 11 to 14) are lower than the values obtained with no end plates. This is probably because of end effects, since end effects (at least for C_{p_b} and, by analogy for C_L') seem to be more extensive near end plates than near gaps, (see e.g. fig. 28).

3.2 EFFECT OF ASPECT RATIO

As already mentioned, the average force over a span of the 'live' section is expected to become smaller as the span gets longer, because the correlation of the force averaged over the body reduces with span. Fig. 11 shows the measured results for the square section in low turbulence. The expected decrease in C_L' occurs only for larger spans, here for $L/H \geq 2$. For the lowest span length, $L/H = 1$, the effect

of gaps between the 'live' section and the end pieces causes a significant reduction in the measured C_L', an effect much more important in the short sections than in those of larger span. As the free stream turbulence increases , the decrease in C_L' with increasing span becomes less pronounced. Figs. 11 to 14 illustrates this idea. Apparently, turbulence makes the fluctuating side forces act more evenly over the span. Put another way, turbulence improves the spanwise correlation of the fluctuating side forces on the square section. One of the reasons for this is that, in turbulence, the shear layer separating from the front corners of a square section, interacts significantly with the after body and causes the forces to act evenly over the span; even when the span is large this interaction apparently remains quite uniform, since the averaged coefficient of the fluctuating side force decreases only very slowly with increasing of span.

An analytical framework for the effect of aspect ratio on the fluctuating lift coefficients, can be developed from the rather simple assumption, that the relevant correlation coefficient has a simple exponential form. With this assumption, the r.m.s. lift force per unit length averaged over a span L and non-dimensionalized to produce a lift coefficient becomes:

$$C_L' = C_{L_o}' \sqrt{2}\lambda/L[L/\lambda - 1 + \exp(-L/\lambda)]^{1/2}$$

where λ is the integral length scale of the force correlation averaged over the span, L is length of the 'live' section, C'_{L_0} is the fluctuating lift coefficient measured locally and C'_L is the fluctuating lift coefficient averaged over the span. See appendix C for details of the derivation. Fig. 15 shows typical measured values of C'_L and the plot of the above equation for selected values of λ/H, C'_{L_0} chosen to fit the data at large L/H. The end effects which include the definition of Δ are discussed in section 3.5.

Present results are like those previously reported for low turbulence, for C'_{L_0} and λ/H (see Tables 1 & 2). For increasing intensity, however we find that λ/H increases, in contrast to previous reports (e.g. ref. 1). A possible reason for the difference between the trends in ref. 1 and those reported here is that, the values reported in ref. 1 are measured using pressure taps while the values reported here are obtained using the average of the force over the 'live' section.

3.3 EFFECT OF TURBULENCE INTENSITY

When the turbulence intensity increases, it moves the oscilating shear layers closer to the sides of the body from which they separate, shortens the unsteady bubble between the separation and reattachment and so progressively reduces the fluctuating side force on the body. Figs. 16 to 20 show the coefficient of fluctuating lift for different levels of

turbulence intensity. It is observed that turbulence always reduces the averaged r.m.s. lift coefficients on square cylinders (if no end effects are present), by disturbing the regularity and spanwise correlation of shedding.

The fluctuating lift for the square section shape varies with free stream turbulence in a similar way to that of the base pressure. Fig. 21, comparing measurements of the base pressure and the fluctuating lift coefficient for different levels of turbulence for one length of the square section, confirms this idea. The similarity appears for all lengths of the square section.

Figs. 22 to 25 show the effect of turbulence intensity produced behind a rod for different aspect ratios. The same pattern is evident as for the case of grid turbulence, but the values are not the same. This is maybe because of the different structure of turbulence generated behind a rod compared to that from a grid, or differences in end effects. Fig. 26 shows a comparison between C_L' measured using a grid and C_L' measured using a rod as turbulence generating devices.

3.4 EFFECT OF LENGTH SCALE

Significant effects of turbulence scale on the drag of bluff bodies have been reported by Lee[20] and Miyata & Miyazaki [21]. However, most authors report no effect of turbulence scale on mean forces over the range $.2<L_x/H<18$. (e.g. see Pety[22] and Laneville & Williams[23]). Gartshore[5]

reports no effect or little effect of turbulence scale on fluctuating forces, provided $L_x \leq H$. A comparison between measured fluctuating lift coefficients for two different integral turbulence scales was made. For two model positions downstream of the test section, two grids one with mesh size of M=.256in(6.5mm) and the other with mesh size of M=4.5in(114.3mm), were used to produce the same level of turbulence intensity (4%) and two different length scales of .179in(4.55mm) (L_x/H=.119) and 1.6in(40.64mm) (L_x/H=1.067) respectively at the front face of the model. No uniform trend in the averaged fluctuating lift coefficient was observed for the two different integral length scales generated. Fig. 27 shows the effect of integral length scale on C_L'.

3.5 END EFFECTS

End effects are particularly important in two dimensional experiments on bluff bodies, since separation regions are easily altered by slight changes in pressure or cross flow far from the centre span.

To remove the effect of the tunnel boundary layer, two end plates were used. Obasaju[18] showed the effect of different end plates on the mean base pressure of a square section. A set of end plates (see fig. 7) specified by Obasaju for square sections, was used without exploring their effectiveness; again absolute values are unlikely to be as important as trends in the present context. Boundary

layers on the end walls confining the cylinder under test may be modified as the free stream turbulence is changed. Some of these problems are discussed by Lee[19] and many experimental studies report concern over the observed sensitivity to end effects.

The other end effects present in this experiment were the gaps between the 'live' section of the model and the adjacent dummy end pieces. The gap was always kept less than .02in(.5mm) for the main experiments. Fig. 28 shows the effect of gap size on the mean base pressure coefficient. As can be seen from the figure, when the gap size gets bigger, the absolute value of the pressure coefficient decreases. If there is a similarity between the base pressure coefficient and the coefficient of fluctuating lift, C_L' will also decrease as the gap size increases. This end effect will be more noticeable in the short span models, so that C_L' for the smallest model (1.5in(38.1mm) length) is lower than for the 3in(76.2mm) model, despite the opposing trend coming from their different aspect ratios . To investigate the effect of gaps, end plates similar to those used near the tunnel walls on the dummy end pieces were tried at both ends of the 'live' section leaving the same gap (<.02in(.5mm)) with the adjacent dummy pieces. In this case also the end plates on the 'live' section produced another effect which again is shown as change of base pressure coefficient near to the end plates in fig. 8.

It was noticed that end effects are less present in high turbulence flows than in low turbulence flow; this shows that turbulence reduces the effects of the ends. Comparing fig. 11 (C_L' for low turbulence) to fig. 14 (C_L' for high turbulence) confirms this matter. Also turbulence reduces effect of gaps on base pressure (see fig. 28).

An analytical framework for the end effect can be developed to modify that developed for the effect of aspect ratio. For this purpose, it is assumed that the end conditions (gaps, end plates, etc.) result in an effective span $(L-2\Delta)$ slightly less than the actual live span L. Therefore, the r.m.s. lift force per unit length averaged over a span L and non-dimensionalized to produce a lift coefficient becomes:

$$C_L'=C_{L_o}'\sqrt{2}\lambda/L[L'/\lambda -1+\exp(-L'/\lambda)]^{1/2} \qquad \text{where } L'=L-2\Delta$$

Apendix C has a derivation of this equation.

Measured results can be fitted by an equation of the above form to infer effective values of λ, Δ and C_{L_o}' for each test.

Typical measured values of C_L' are shown in fig. 15, where the above equation is also plotted for selected values of λ/H, C_{L_o}' and Δ/H. In this way, values of the three parameters for all tests are found. These are summarized in Table 2. Values of C_{L_o}' are shown in fig. 29. These values are extrapolations of C_L' curves (averaged over the span) as

a function of L/H to a value for L/H≃0 (corrected for end effects). These values are not certain in some cases, because of the scatter of C_L' (averaged over the span) for some 'live' sections. For comparison, local values of C_L' (C_{L_0}') measured by others are also plotted in fig. 29. Gartshore[5] used a rod as the turbulence producing device for the turbulence values presented in fig. 29, while Lee's[3] turbulence values and the present data are measured using grids as the turbulence producing devices. As noted earlier, when the turbulence intensity increases, λ/H increases and the ratio Δ/H, representing end effects, decreases showing that end effects become less significant as the intensity increases. In fig. 29, the present values of C_{L_0}' for square sections (B/H=1) are quite agreable with the literature. However, the values of C_{L_0}' for other sections (B/H=.67 and B/H=.50) are different than the values reported by Gartshore[5] although the trends are similar. The difference is perhaps because of the different methods of measurements, different turbulence producing devices, different blockage ratios and different end effects.

4. RESULTS FOR OTHER SECTION SHAPES

4.1 RECTANGULAR SECTION WITH B/H=.67

For this rectangular shape, C_L' for each live span was found at various wind speeds and turbulence intensities as was done in the square section case. The values of C_L' found for this section shape did not show such clear trends as for the B/H=1 section, and values over a reasonable speed range were not as constant. In some cases, the values were scattered between ±.4 of the quoted values. Despite this uncertainty in the values, some conclusions can be drawn. As is shown in fig. 30 to 33, C_L' decreases very slowly with aspect ratio. Although the trend is not as clear as for square sections, it is evident that C_L' changes slightly with turbulence intensity for all spans. The effect of integral length scale was tested on the longest span of this rectangular shape, and as it is shown in fig. 27, there seems to be no effect of turbulence length scale on the fluctuating lift coefficient over the range tested. Looking at the results obtained for the base pressure (fig. 34), the effect of the gap is again more present in the low turbulence stream than in higher turbulent flow. It also shows that the end effect (because of gaps) may be slightly changed with Re, since the base pressure coefficient trend near the gap has changed slightly for the two different Re used. This is perhaps one of the reasons why the values of C_L', in some cases, are different for different speeds.

4.2 RECTANGULAR SECTION SHAPES WITH B/H=.5

For this rectangular shape also, C_L' for each span was found at different speeds as was done for the other rectangular sections. C_L' for each 'live' section at different levels of free stream turbulence intensity was deduced as before. Figs. 35 to 38 and fig. 29 show that there is almost no significant change of C_L' with turbulence intensity for any of the spans tested. The reason for this is that, as the turbulence intensity increases, the rear corner of the body which was interfering with the separating shear layer of the square section interferes in the second rectangular section (B/H=.67) and has very little effect on the afterbody of the rectangular section with B/H=.5 in the range of turbulence levels used. Therefore, the turbulence level makes very little change to the value of C_L'. However, figs. 35 to 38 show that C_L' decreases as the aspect ratio gets larger. Although this trend is not as clear as it was in the case of square sections, it demonstrates again that C_L' is less correlated for longer bodies than for shorter bodies, as expected. The effect of integral length scale was tested on the longest span of this rectangular shape, and as is shown in fig. 27, there seems to be no essential change in C_L' with change in length scale, over the range tested.

4.3 COMPARISON FOR ALL SECTION SHAPES

Comparing the overall variation of C_L' with turbulence intensity in the rectangular sections (ignoring the end effects), it can be concluded that as the turbulence intensity increases, C_L' decreases in square sections. For sections with B/H=.67 this decrease of C_L' with turbulence intensity is lower than that for the square sections. For sections with B/H=.5, C_L' first rises with increase of turbulence intensity and then drops as the turbulence intensity is further increased.

Looking at the variation of C_L' with aspect ratio, there is one trend evident in all the three rectangular sections and that is: C_L' always decreases with an increase of aspect ratio, L/H (excluding end effects), no matter what the level of the turbulence intensity is. In any level of turbulence intensity, the unsteady lift per unit length depends upon section shape.

5. CLOSING COMMENTS

5.1 CONCLUSIONS

The objectives of this test were:

1- To investigate the effect of turbulence on the fluctuating lift forces induced by vortex shedding on two dimensional rectangular cylinders.

2- To investigate the effect of span or aspect ratio (L/H) on the averaged fluctuating lift forces imposed on the body.

The section shapes used are of importance because they are particularly sensitive to free stream turbulence effects. Literature has shown (see e.g. Gartshore[5]) that rectangular sections with B/H>1 have a more permanent reattachment of the separating shear layers to the sides of the body, in turbulent flow, and the magnitude of C_L' is relatively small.

For square sections, an increase in turbulence intensity decreased C_L', the decrease being greater for the small span models than for the large ones. For sections with B/H=.67 this decrease was slower and for sections with B/H=.5, C_L' increased first and then decreased very slightly. C_L' measured for square sections using a rod as the turbulence producing device, in all cases, showed a lower value than the C_L' measured using a grid as the turbulence

producing device for the same intensity. This is probably because of the different structures of turbulence behind a grid and a rod. See fig. 27 for comparison of grid data and rod data. The effect of turbulence scale was checked on the rectangular sections and there was no clear trend observed for the range of the scales used.

C_L' decreased with increasing span of the 'live' section in all the rectangular shapes except for the small span that was extensively affected by end conditions. End conditions were more obvious in the small spans than in large ones. End effects were less significant in high turbulence intensity than in low turbulence levels, an effect observed on C_L' and mean base pressures.

5.2 COMMENTS ON THE EXPERIMENTAL METHOD USED

The advantage of using a single beam as a force transducer is that the beam is simple to make and to use, and is very inexpensive, avoiding other force or pressure transducers. It also measures force directly over a range of forcing frequencies.

End conditions play an important role in the data, and gaps must be left at the ends of the live section, necessarily introducing complicated (although realistic) end effects. In addition, because of the increasing mass of the larger sections, the range of speeds or forcing frequencies that can be used is progressively decreased. Vibration amplitude, although always small in these tests, could

introduce further variables in some cases.

For strictly 2D tests, two related effects must be investigated: the end plates used must be shown to be effective so that 2D flow is produced and the end gaps necessarily present in the present tests must be eliminated. For the first effect, end plates of various sizes need to be studied with sections of each geometry, perhaps in conjunction with various turbulence levels and various blockage ratios. End gaps might be sealed with a suitable gasket or sealing ring and could be avoided altogether if many pressure taps were used, perhaps connected to suitable manifolds.

Finally, a wide range of B/H could be considered, and greater accuracy, to be more certain of trends, would certainly be desireable.

BIBLIOGRAPHY

1. Vickery, B.J.
"Fluctuating lift and drag on a long cylinder of square cross section in a smooth and in a turbulent stream.", J.F.M. 25, 1966, pp 481 to 494.

2. Pocha,J.J.
Ph.D. thesis, Department of Aeronautical Engineering, Queen Mary College,1971.

3. Lee, B.E.
"The effect of turbulence on the surface pressure field of a square prism.", J.F.M. 69, 1975, pp 263 to 282.

4. Wilkinson, R.N.
"Fluctuating pressures on an oscilating square prism.", Aero. Quarterly, Vol. 32, Parts I and II, 1981, pp 97 to 125.

5. Gartshore, I.S.
"Some effects of upstream turbulence on the unsteady lift forces imposed on prismatic two dimensional bodies.", J.F.Eng. 106, Dec. 1984, pp 418 to 424.

6. Bearman, P.W. and Obasaju, E.D.
"An experimental study of pressure fluctuations on fixed and oscilating square section cylinders.",J.F.M. 119, 1982, pp 297 to 321.

7. So, R.M.C. and Savkar, S.D.
"Buffeting forces on rigid circular cylinders in cross flows.", J.F.M. 105, 1981, pp 397 to 425.

8. Baines, W.D. and Peterson, E.G.
"An investigation of the flow through screens.", Transactions of ASME, July 1951, pp 467 to 480.

9. Vickery, B.J.
"On the flow behind a coarse grid and its use as a model of atmospheric turbulence in studies related to wind loads on buildings.", National Phisical Lab. Aero. Rep. 1143, March 1965.

10. Campbell,A.C. and Etkin, B.
"The response of a cylinderical structure to a turbulent flow field at subcritical Reynolds number.", UTIAS Technical Note 115, July 1967.

11. Surry, D.
"The effet of high intensity turbulence on the aerodynamics of a rigid circular cylinder at subcritical Reynolds number.", UTIAS Report 142, October 1969.

12. McLaren, F.G. and Sherratt, A.F.C. and Morton, A.S.
"Effect of free stream turbulence on the drag coefficients of bluff sharp-edged cylinders.", Nature 223, No. 5208, August 1969, pp 828 to 829.

13. Laneville, A.
"Effects of turbulence on wind induced vibrations of bluff cylinders.", Ph.D. thesis, University of British Columbia, 1973.

14. Van der Hegge-Zijnen, B.G.
"Measurements of the intensity, integral scale and microscale of turbulence downstream of three grids in a stream of air.", Applied Scientific Research, Section A, Vol. 7, 1958, p.149.

15. Gartshore, I.S.
"The effect of free stream turbulence on the drag of twodimensional prisms.", University of Western Onterio, Faculty of Engrg. Sci. Report BLWT, Oct 1973, pp 4 to 73.

16. Townsend, A.A.
"The structure of turbulent shear flow.", Cambridge University Press, London, 1956.

17. Stansby, P.K.
"The effet of end plates on the Base pressure coefficient of a circular cylinder.", Aer. J., January 1974, pp 36 to 37.

18. Obasaju,E.D.
"On the effect of end plates on the mean forces on square section cylinders .", J. Ind. Aero. 5, 1979, pp 179 to 186.

19. Lee, B.E.
"The susceptibility of tests on two dimensional bluff bodies to incident flow variation.", J. Ind. Aero. 2, 1977, pp 133 to 148.

20. Lee, B.E.
"Some effects of turbulence scale on the mean forces on a bluff body.", J. Ind. Aero. 1, 1975/76, pp 361 to 370.

21. Miyata, T. and Miyazaki, M.
"Turbulence effects on aerodynamic response of rectangular bluff cylinders.", Proc. 5th Int. Conf. on Wind Engineering, 1979, pp 631 to 642.

22. Petty, D.G.
"The effect of turbulence intensity and scale on the flow past square prisms.", J. Ind. Aero. 4, 1979, pp 247 to 251.

23. Laneville, A. and Williams, C.D.
"The effect of intensity and large scale turbulence on the mean pressure and drag coefficients of two dimensional rectangular cylinders.", Proc 5th Int. Conf. on Wind Engineering, 1979, pp 397 to 406.

Author	Method	Model;B/H	r.m.s. lift coef.	u'/U	L_x/H or $L_x/2R$	Live section span L/H or L/2R	Blockage
Vickery	Averaged & extrapolated to local	1	1.32 .68	low 10%	---- 1.33	1/2	7.14%
Lee	Local	1	1.22 1.00 .95 .95 .58	low 4.4% 6.5% 8% 12.5%	---- .97 1.14 .73 .94	---	3.6%
Wilkinson	Local	1	1.35	low	----	---	
Gartshore	Local	2 1 1 1 .67 .50	.41 1.10 .92 .70 1.74 1.76	low low 6% 10% low low	---- ---- $.2<L_x/H<2$ $.2<L_x/H<2$ ---- ----	---	8.3%
Bearman & Obasaju	Local	1	1.20	low	----		5.5%
Pocha	Local	1	1.41	low	----		
So & Savkar	Averaged	circular	$4*10^4<R_e<4*10^5$ .25 to 1.42 $3.8*10^4<R_e<4*10^5$ .20 to 1.35 $3.5*10^4<R_e<3.8*10^5$ .1 to .75 $3.5*10^4<R_e<3.8*10^5$ .08 to .75 $3.2*10^4<R_e<5*10^5$ .1 to 1.05	 10% 10% 10% 10% low	.16 to 1.3 ----	 1 2 3 5.3 3	15.9%

Table 1. Unsteady lift coefficients reported in the literature

	B/H=1			B/H=.67			B/H=.50			
	C_{L_0}'	λ/H	Δ/H	C_{L_0}'	λ/H	Δ/H	C_{L_0}'	λ/H	Δ/H	u'/U
Present Results	1.4	4.8	.08	2.4	6.4	.08	1.6	4.8	.08	.002
	1.3	8.0	.040	2.2	4.8	---	2.0	3.2	>.032 <.13	.04
	1.2	9.6	.032	2.1	6.4	.024	1.6	6.4	.008	.06
	.8	14.4	<.008	1.6	6.4	.008	1.5	3.2	---	.10
Vickery (1967)	1.32 .68	5.6 3.3	--- ---							0 .10

Table 2. Values of λ/H, C_{L_0}' AND Δ/H for rectangular sections

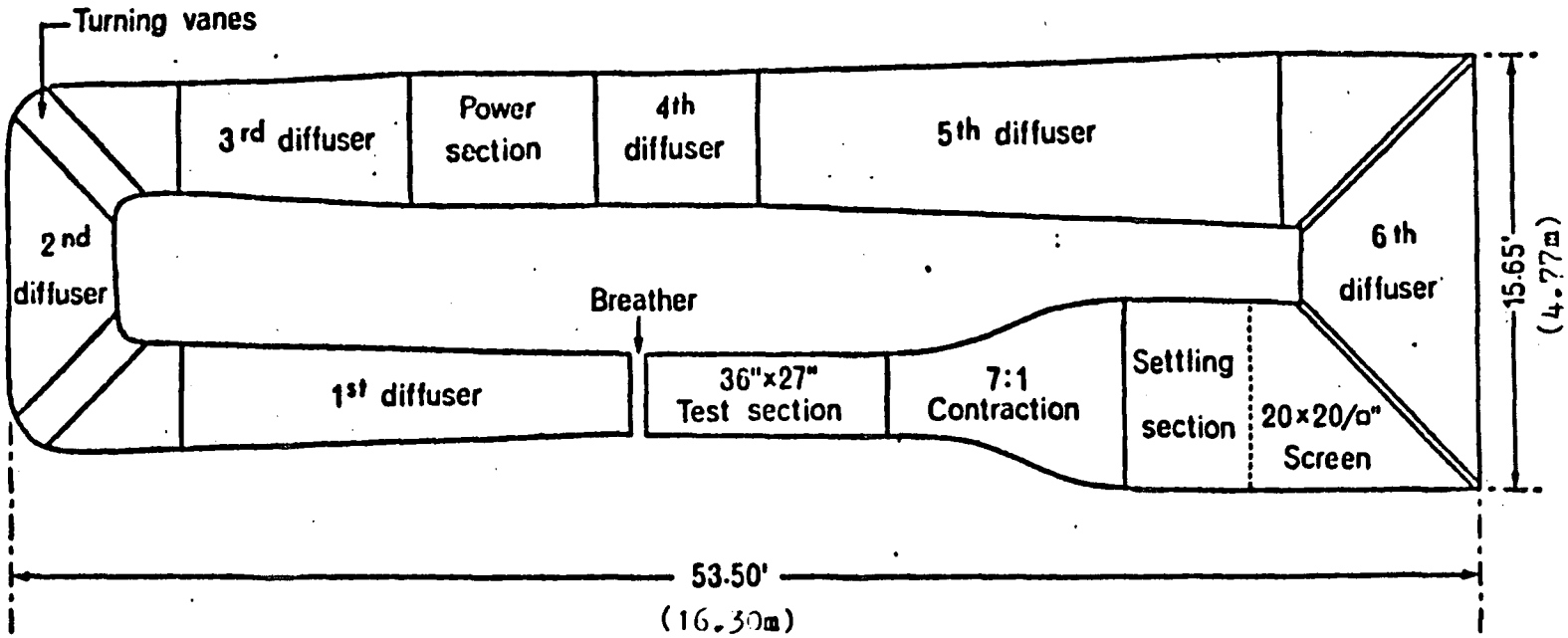

Figure 1: Tunnel outline

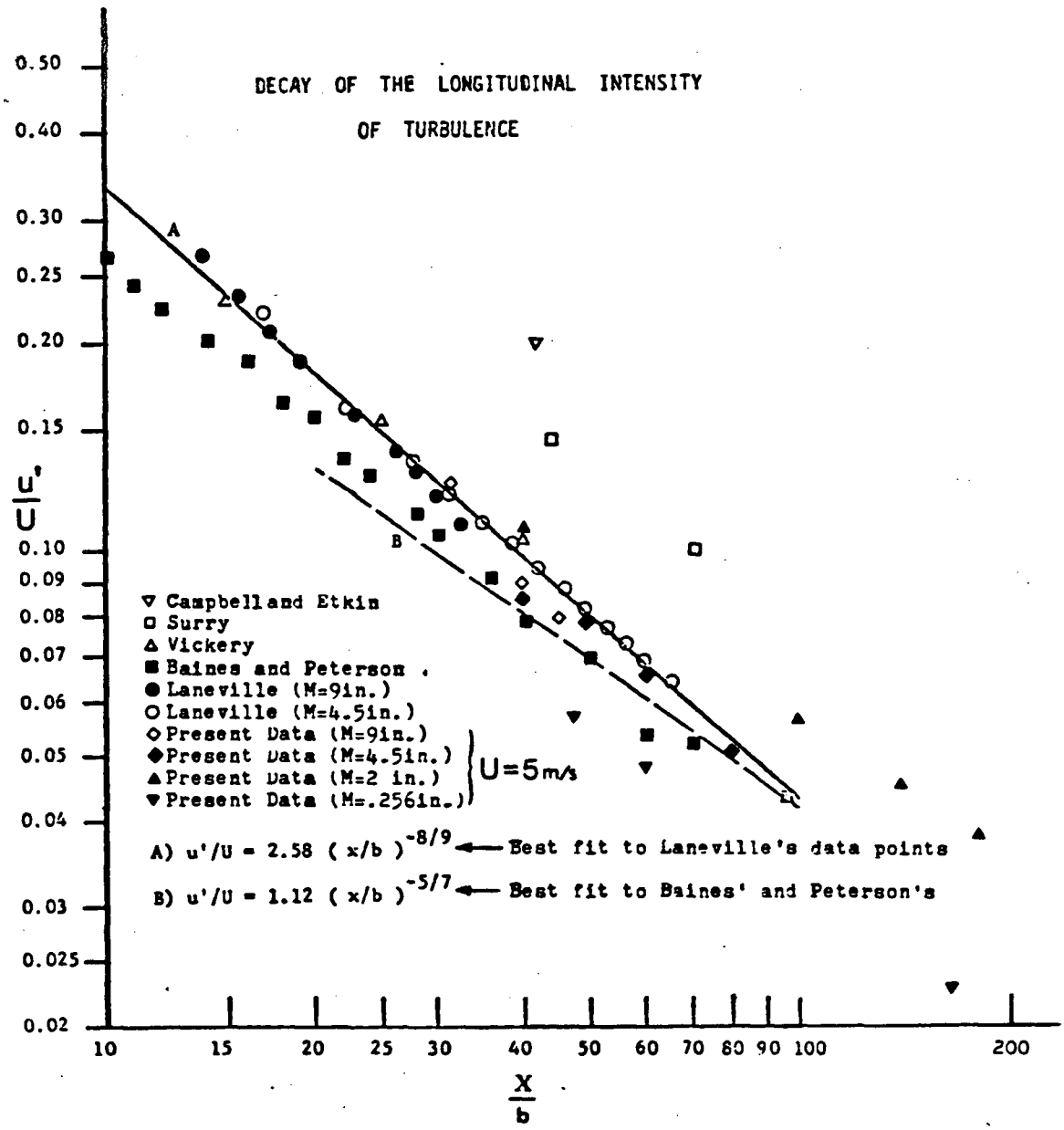

Figure 2: Decay of longitudinal intensity of turbulence

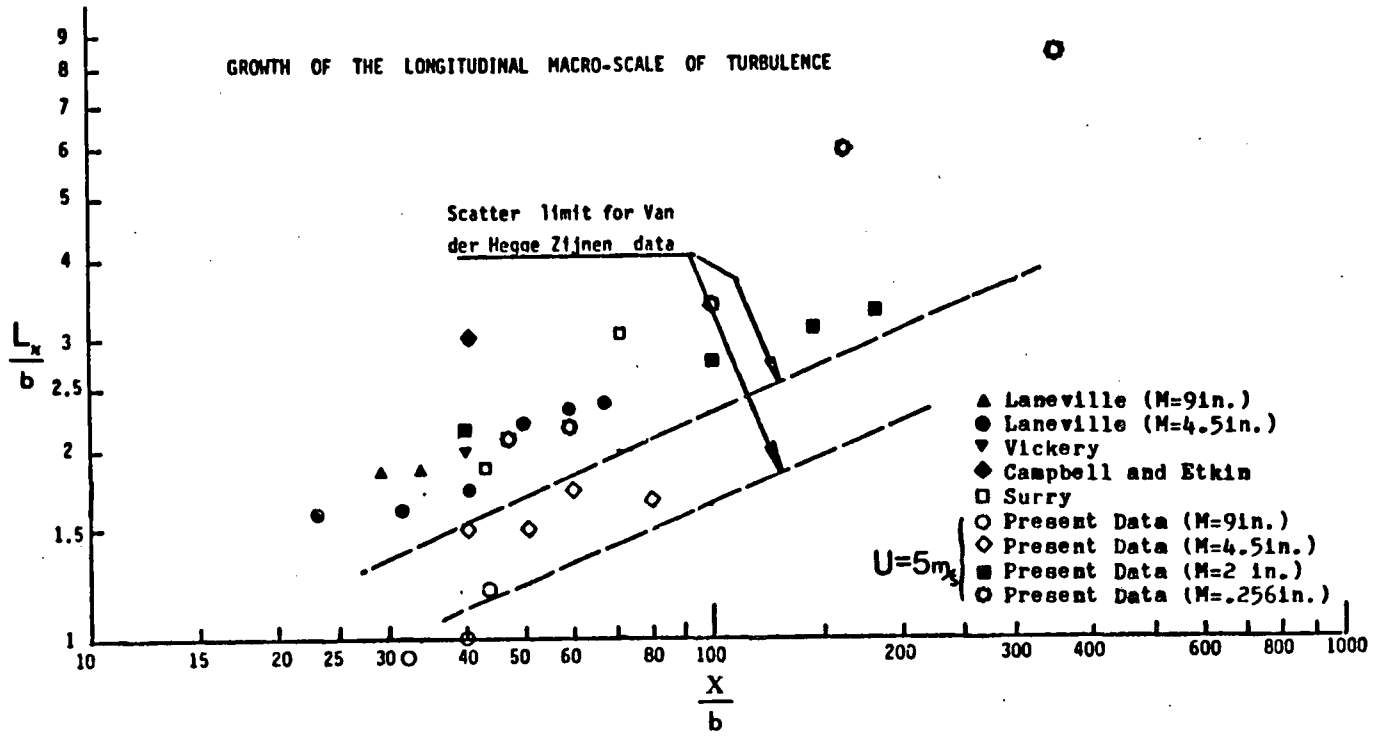

Figure 3: Growth of longitudinal scale of turbulence with downstream distance

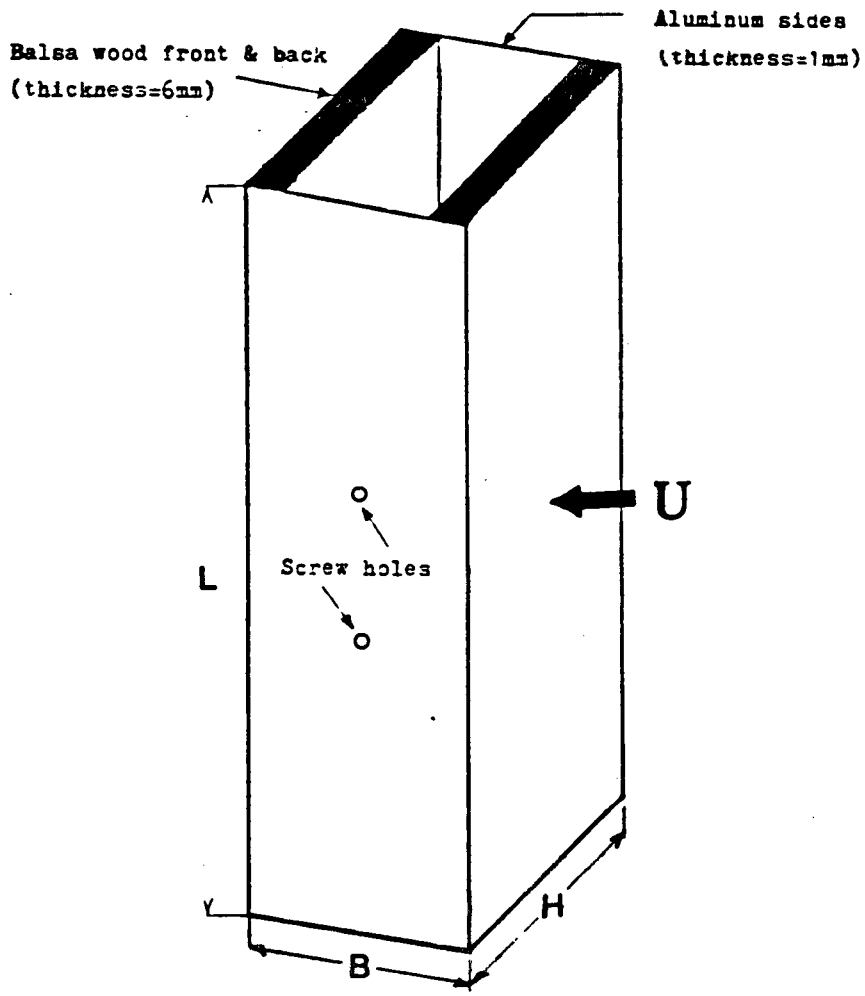

Figure 4: Sketch of a live section

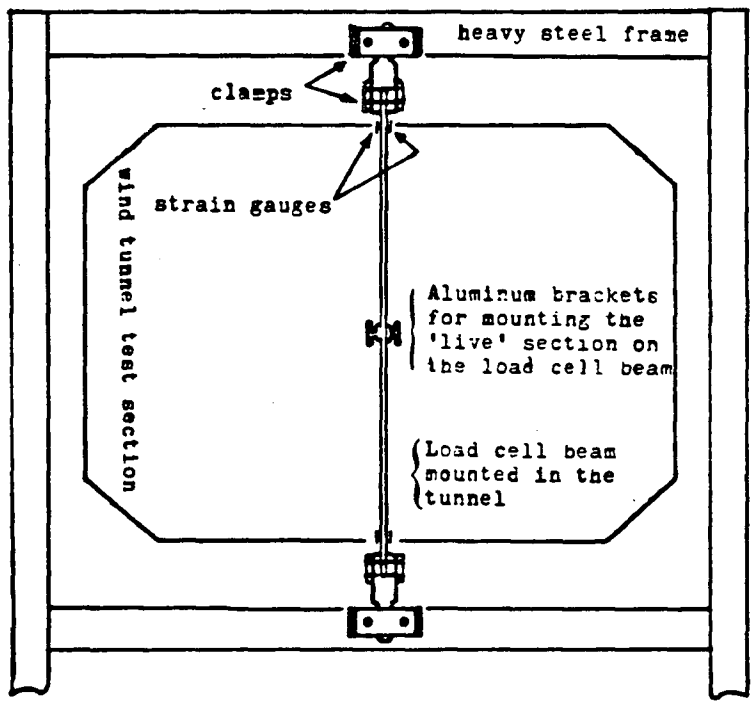

Figure 5: Sketch of the load cell beam

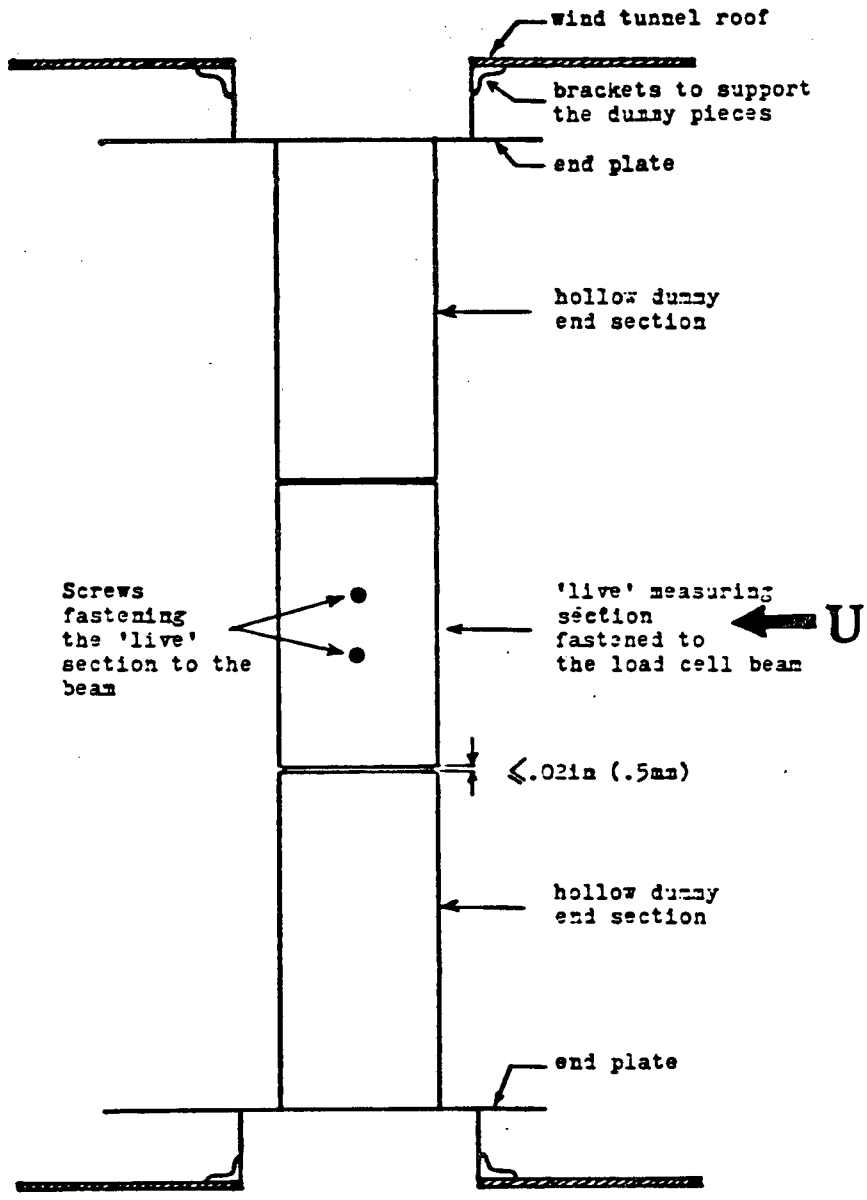

Figure 6: Sketch of a typical model inside the wind tunnel

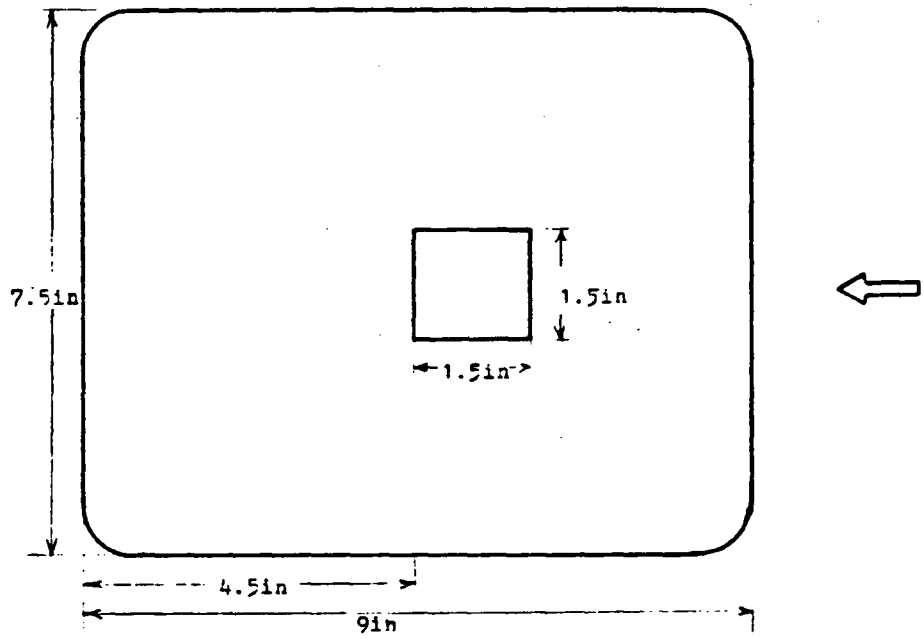

Figure 7: End plates

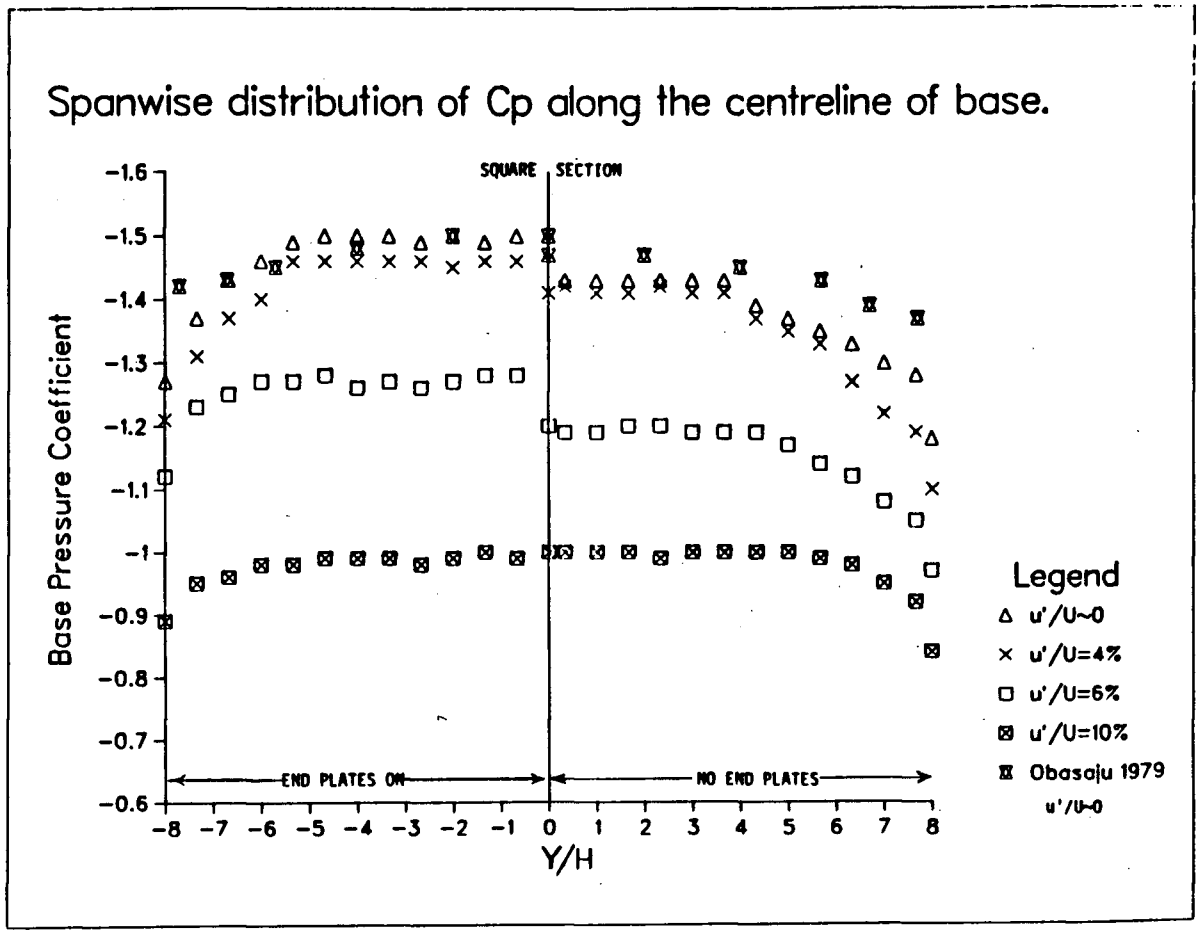

Figure 8: Base pressure coefficints for square cylinders in smooth and turbulent flows.

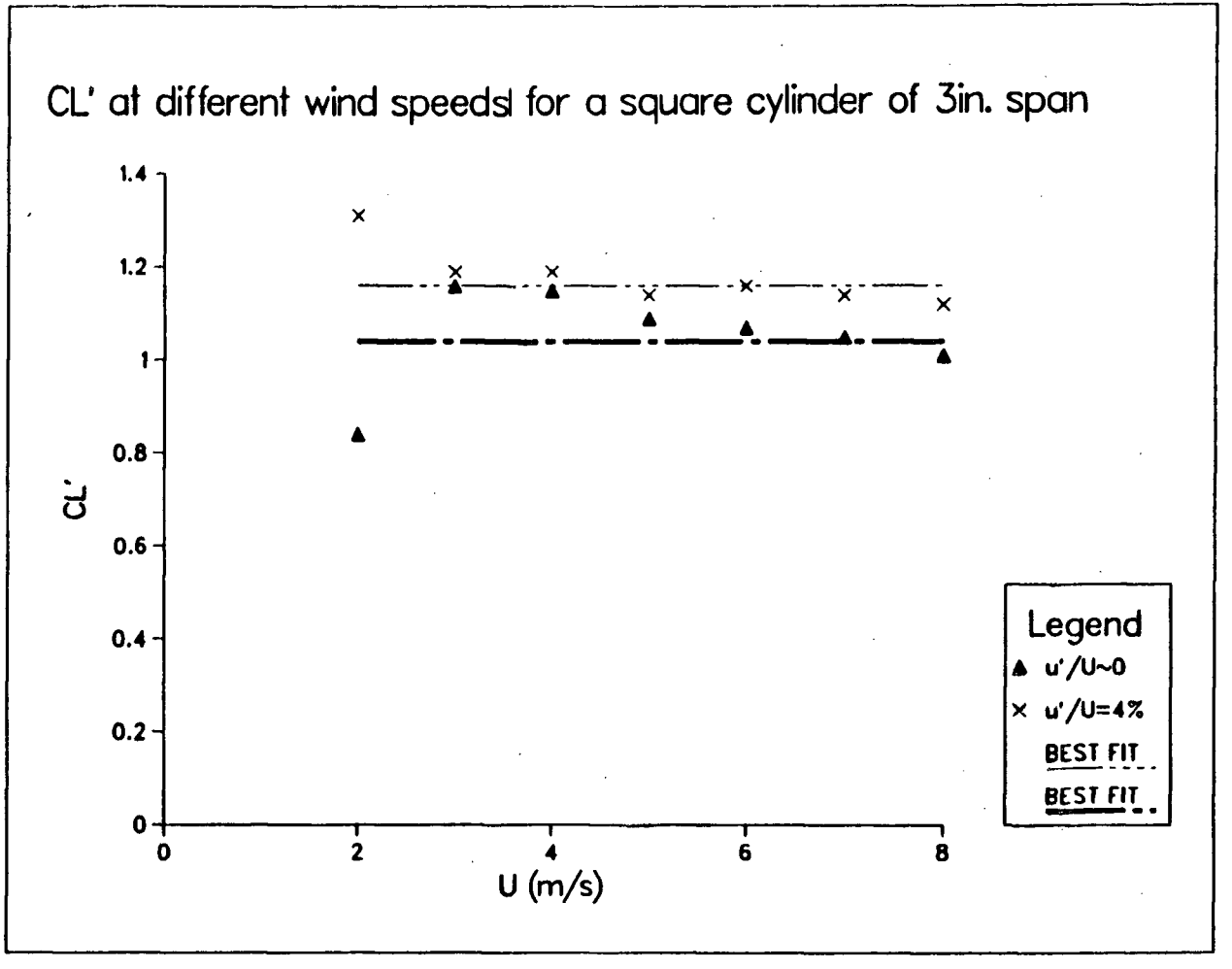

Figure 9: r.m.s. lift coefficients at different wind speeds

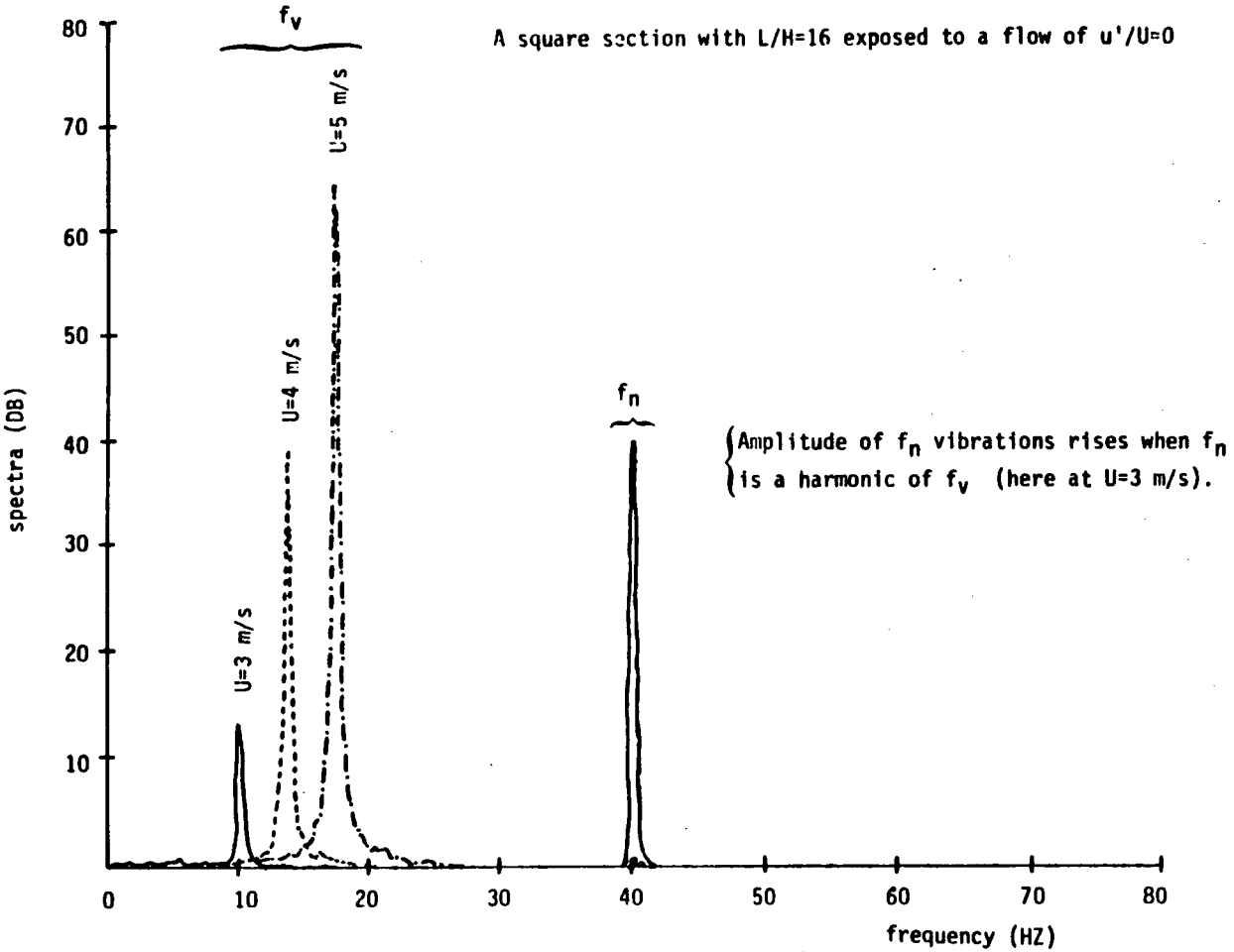

Figure 10: A typical spectrum of the f_n and f_v

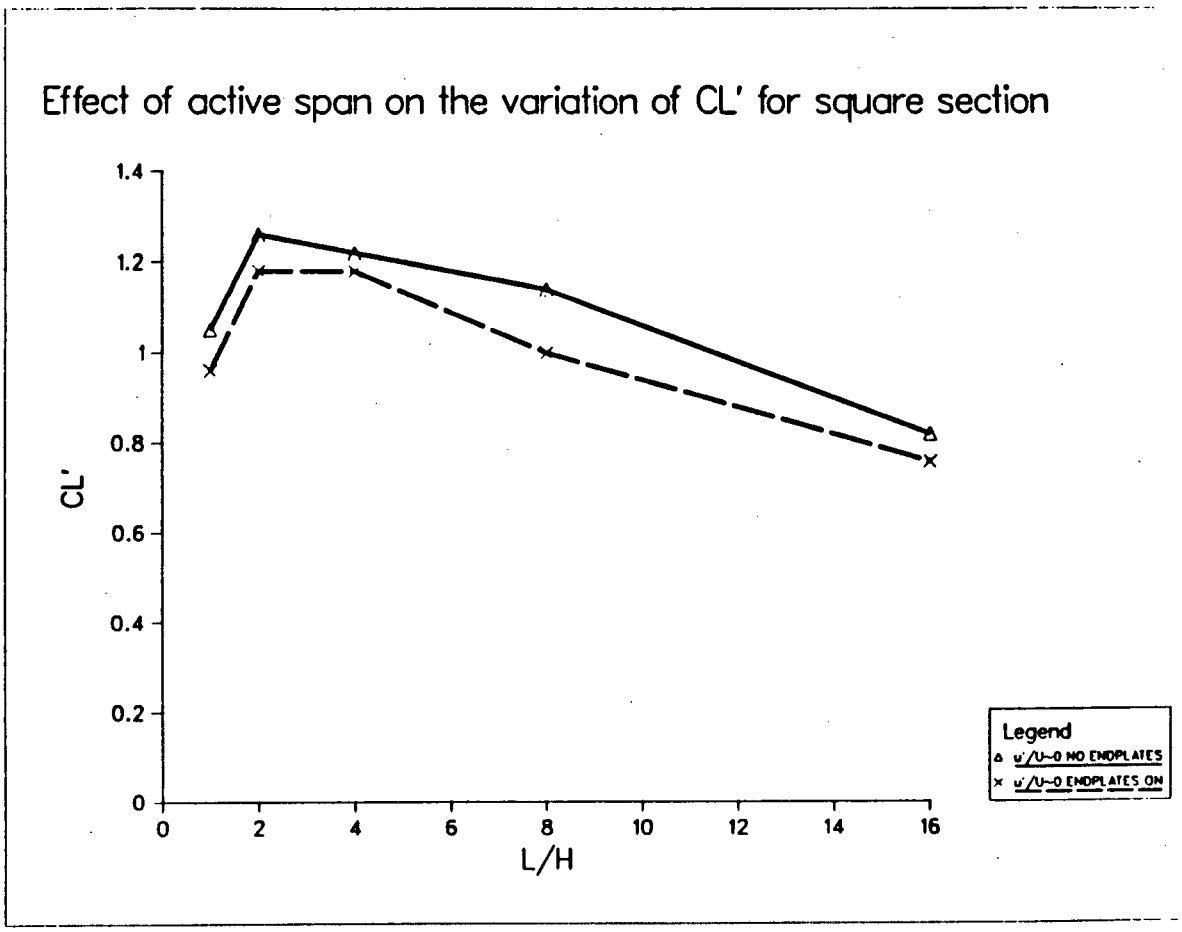

Figure 11: C_L' as a function of aspect ratio for square cylinders at u'/U≃0 (with and without end plates)

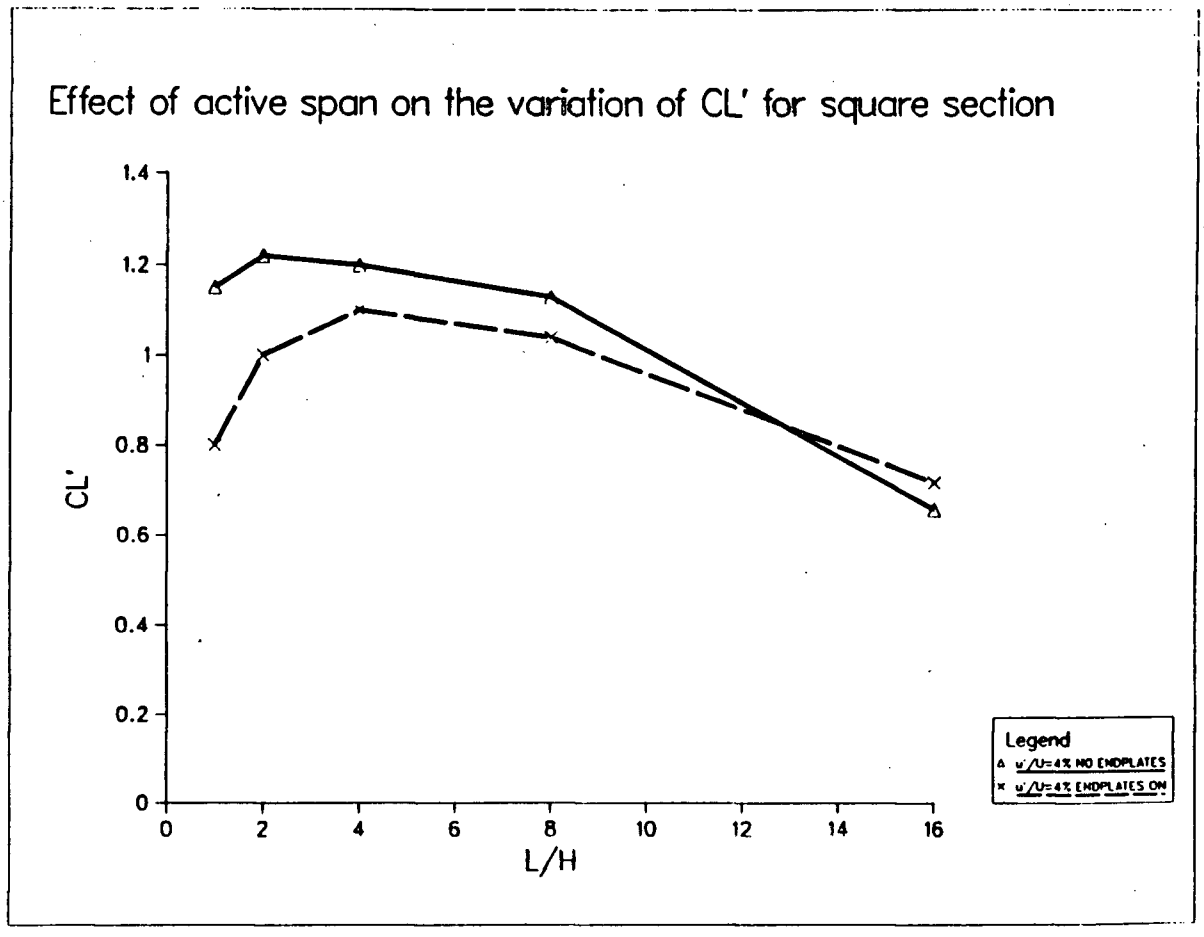

Figure 12: C_L' as a function of aspect ratio for square cylinders at $u'/U=4\%$ (with and without end plates)

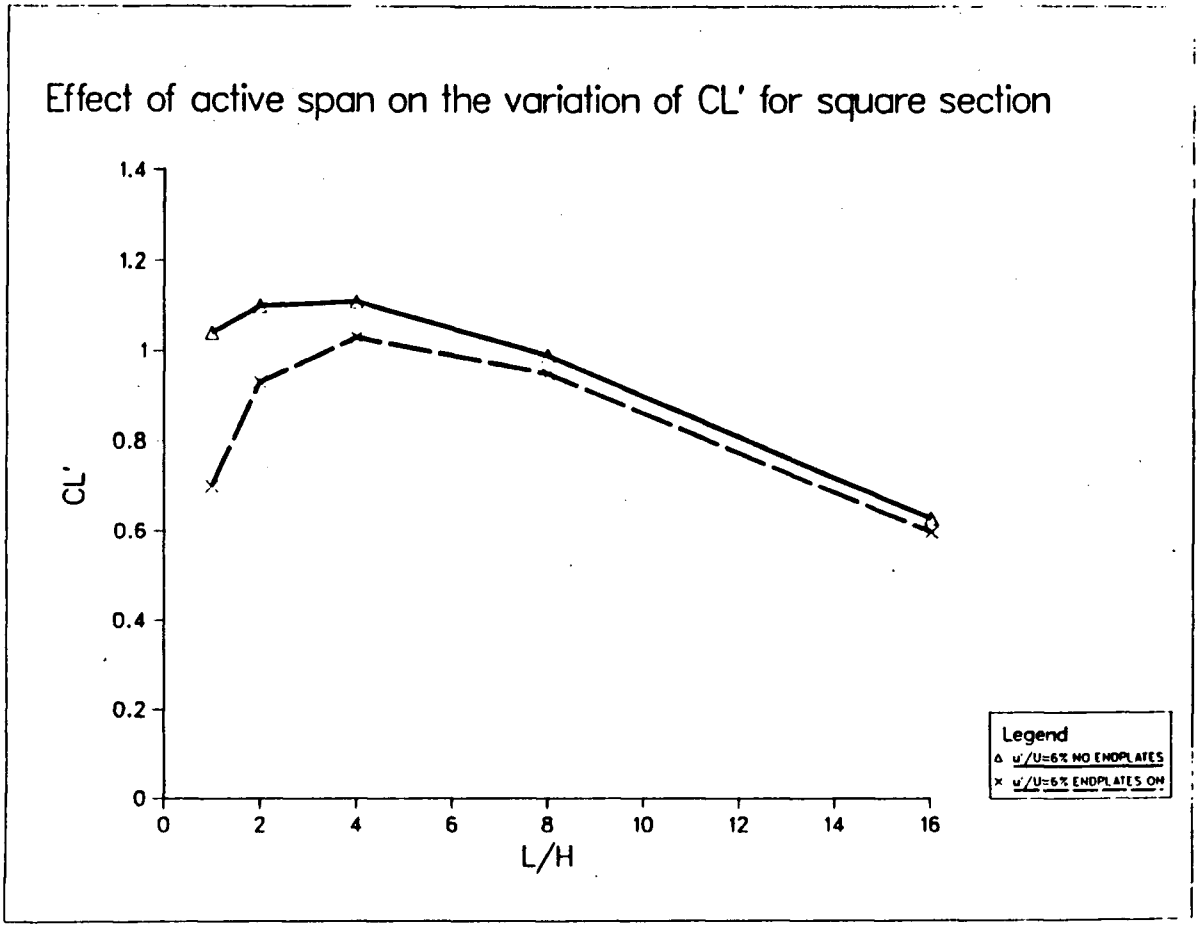

Figure 13: C_L' as a function of aspect ratio for square cylinders at u'/U=6% (with and without end plates)

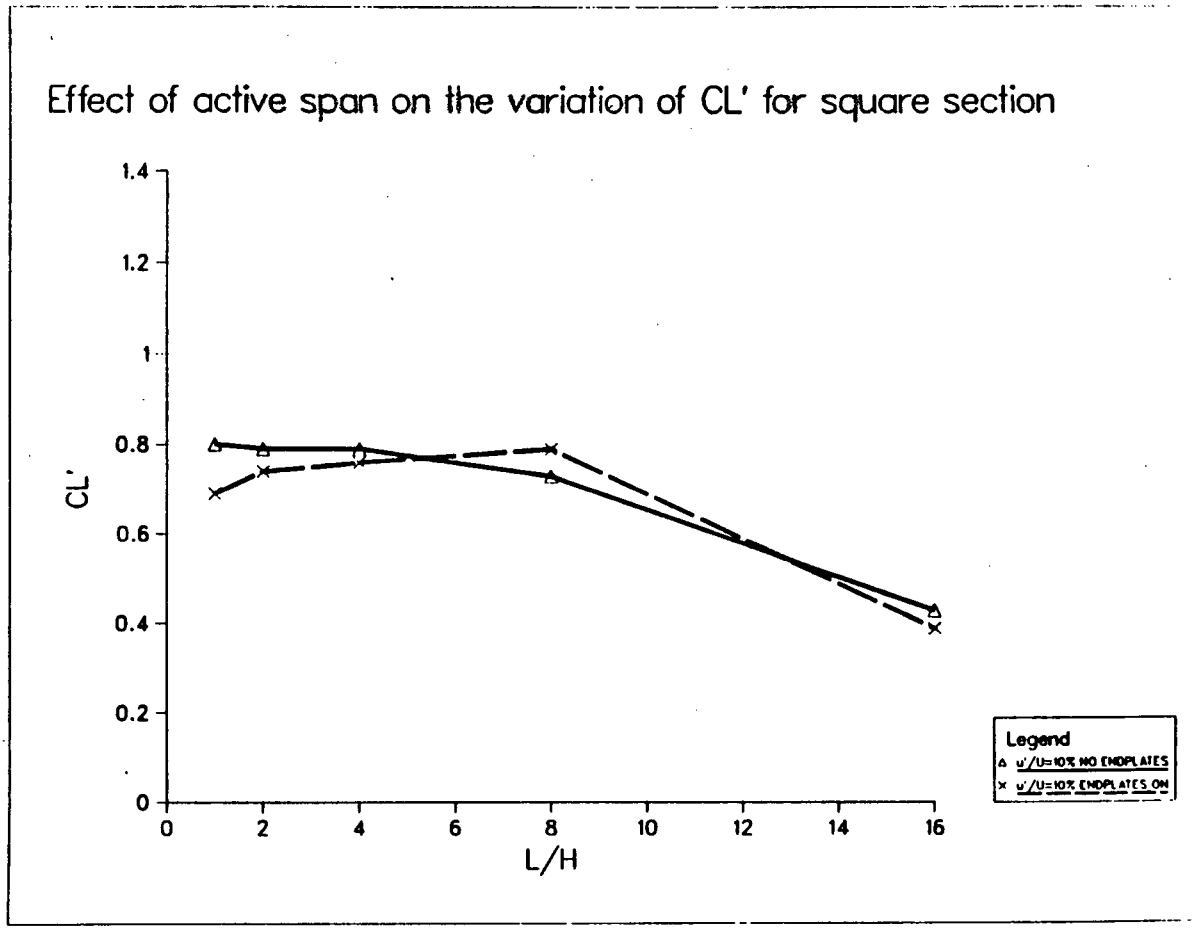

Figure 14: C_L' as a function of aspect ratio for square cylinders at u'/U=10% (with and without end plates)

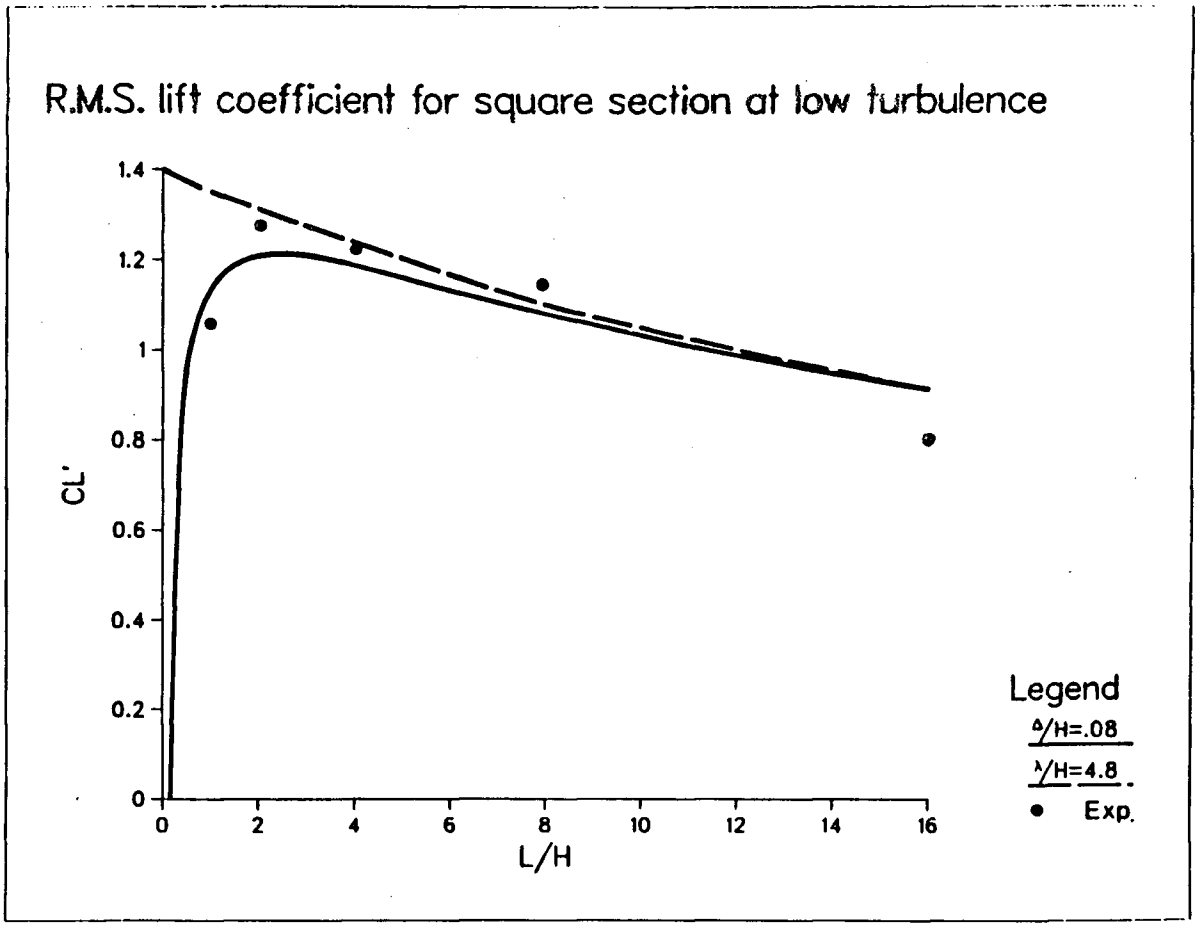

Figure 15: C_L' for square cylinders at u'/U≈0 along with the analytical models

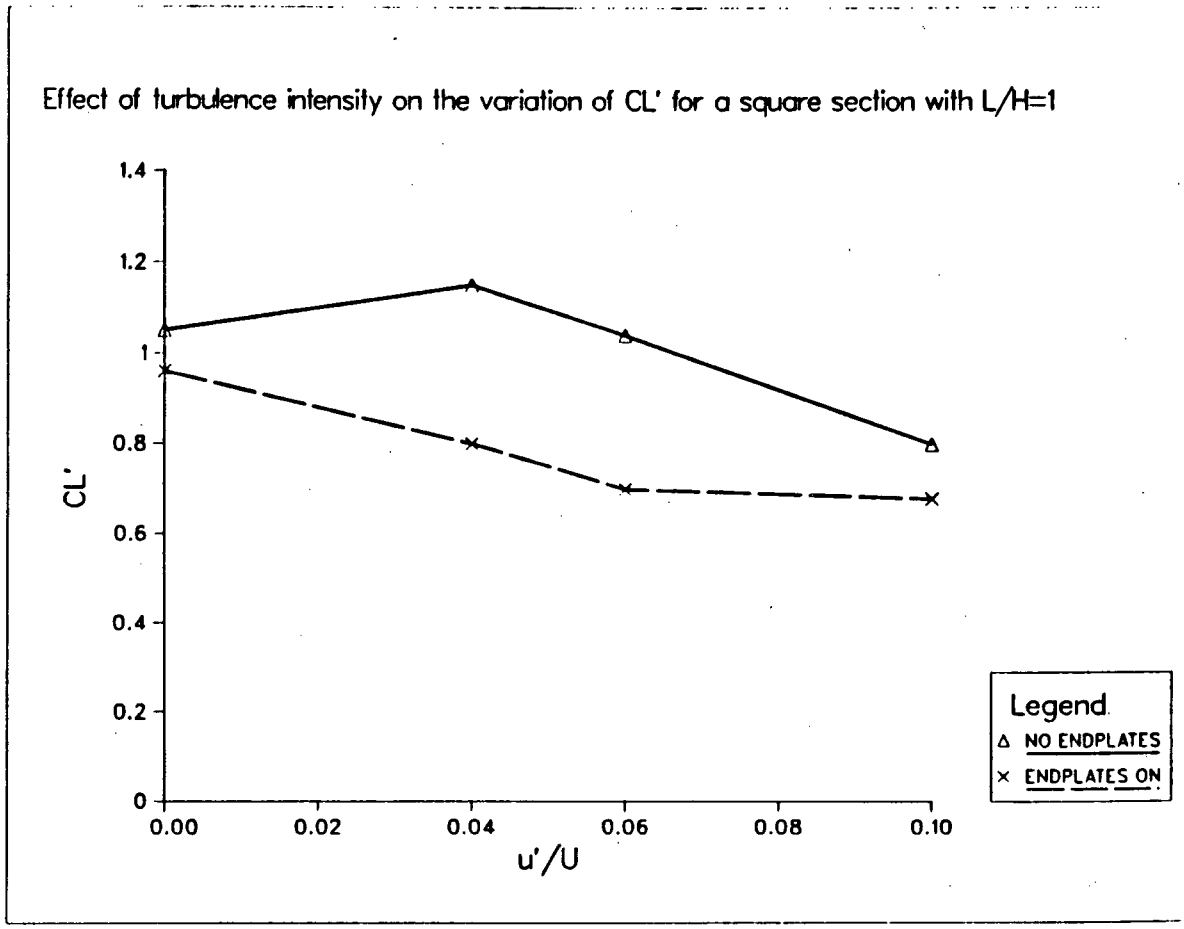

Figure 16: C_L' as a function of intensity for a square section with L/H=1

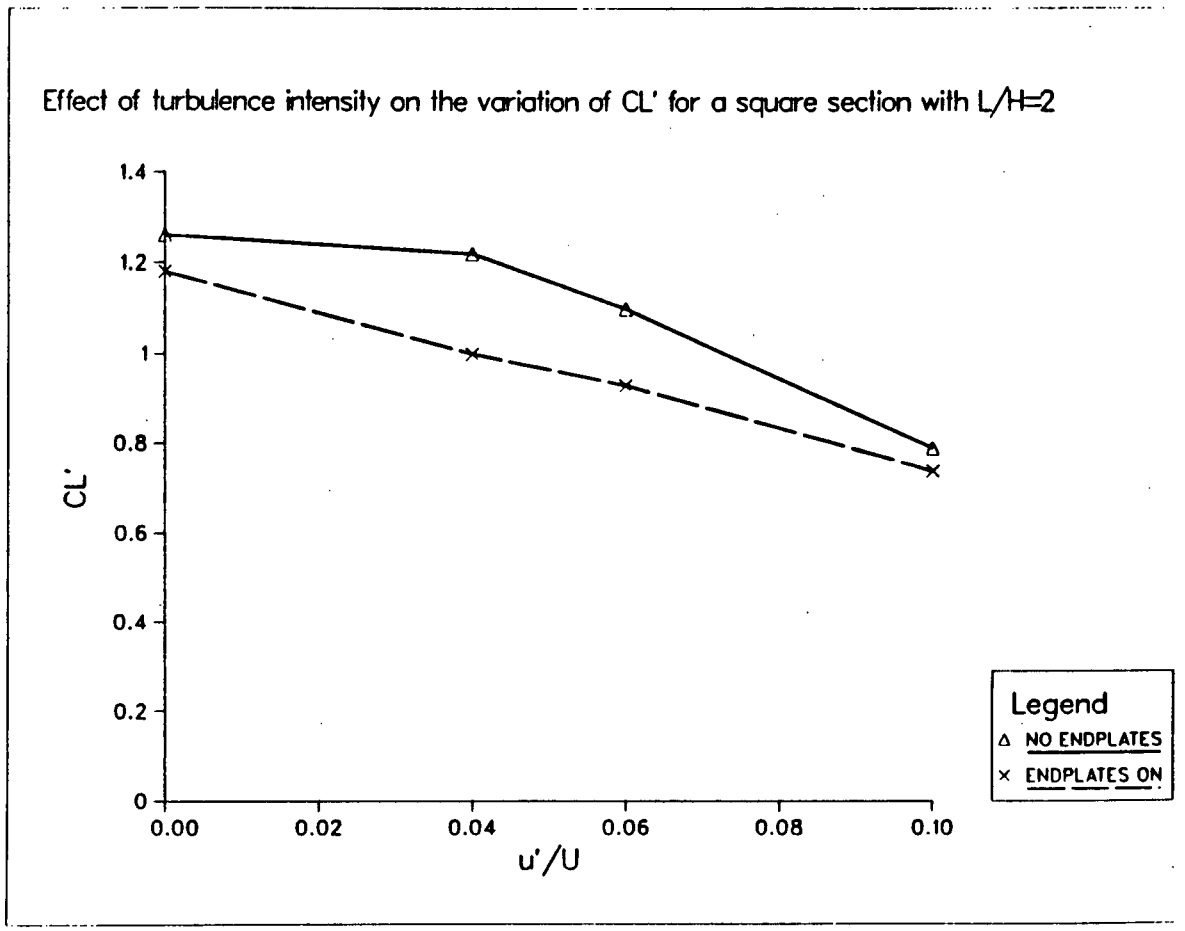

Figure 17: C_L' as a function of intensity for a square section with L/H=2

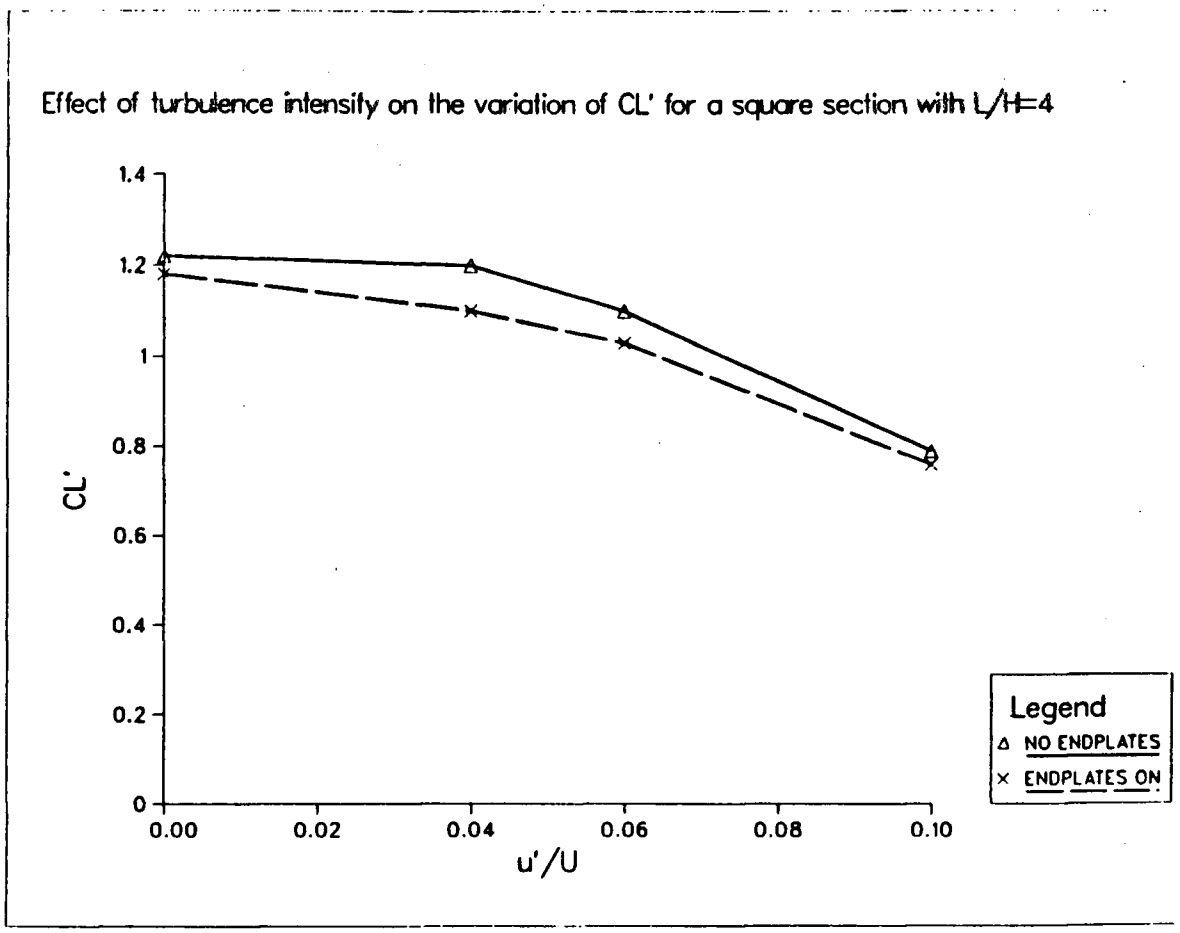

Figure 18: C_L' as a function of intensity for a square section with L/H=4

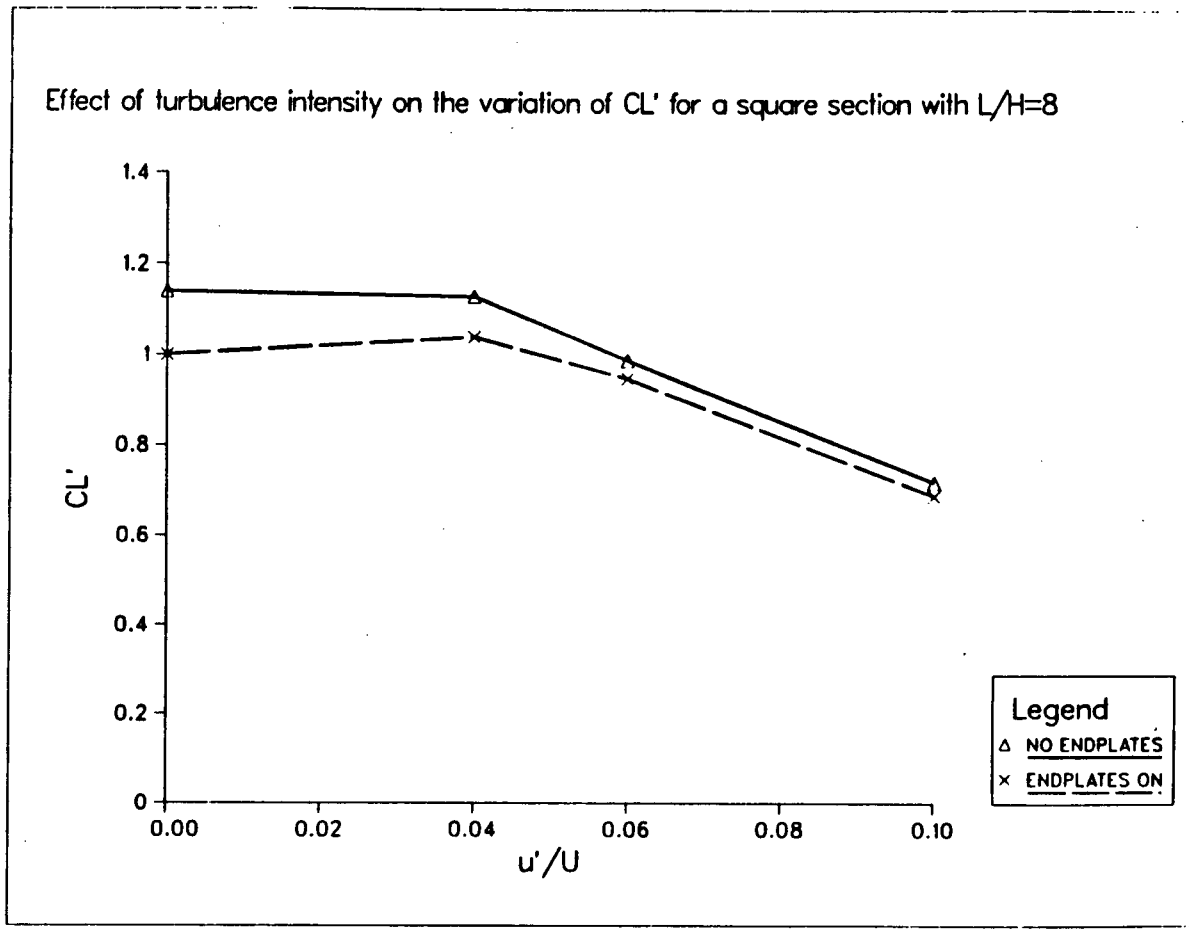

Figure 19: C_L' as a function of intensity for a square section with L/H=8

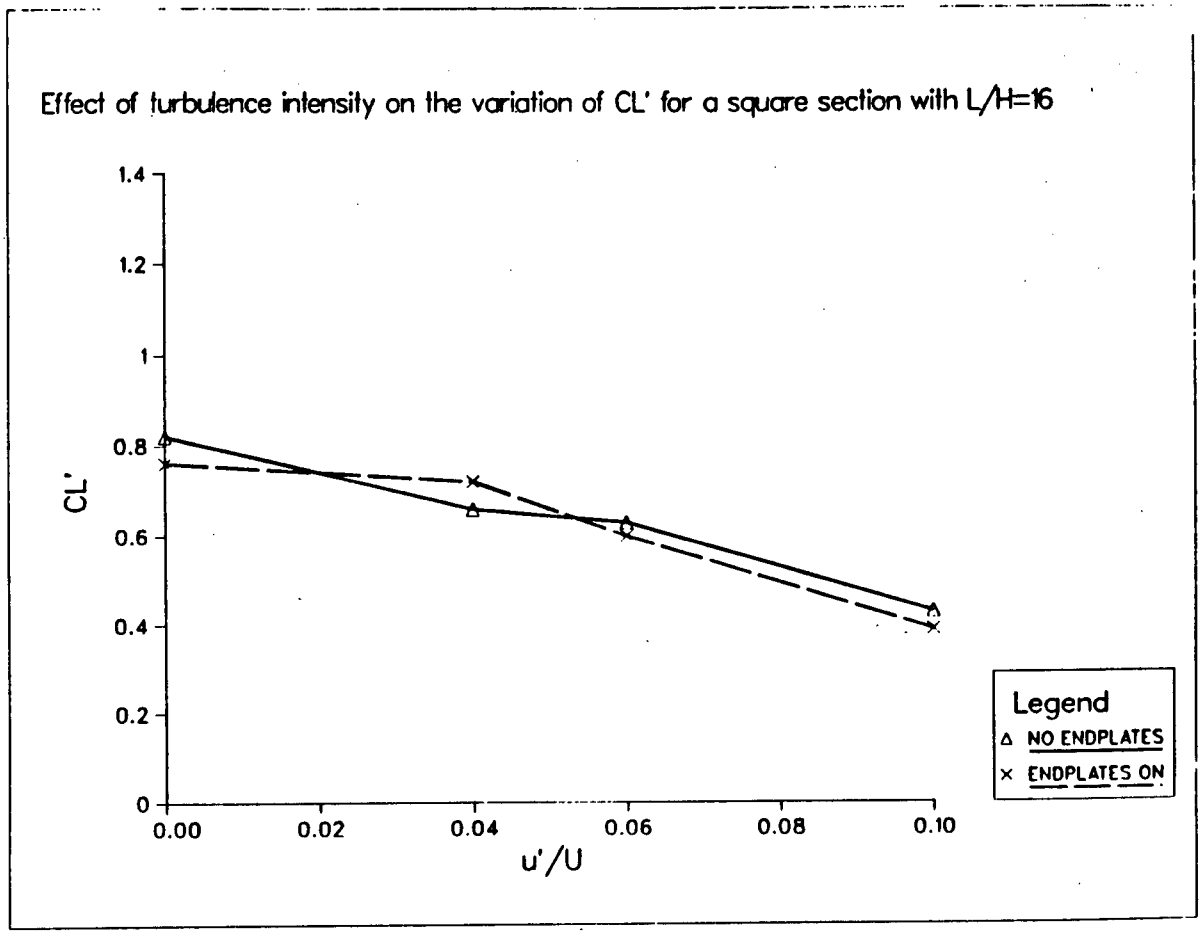

Figure 20: C_L' as a function of intensity for a square section with L/H=16

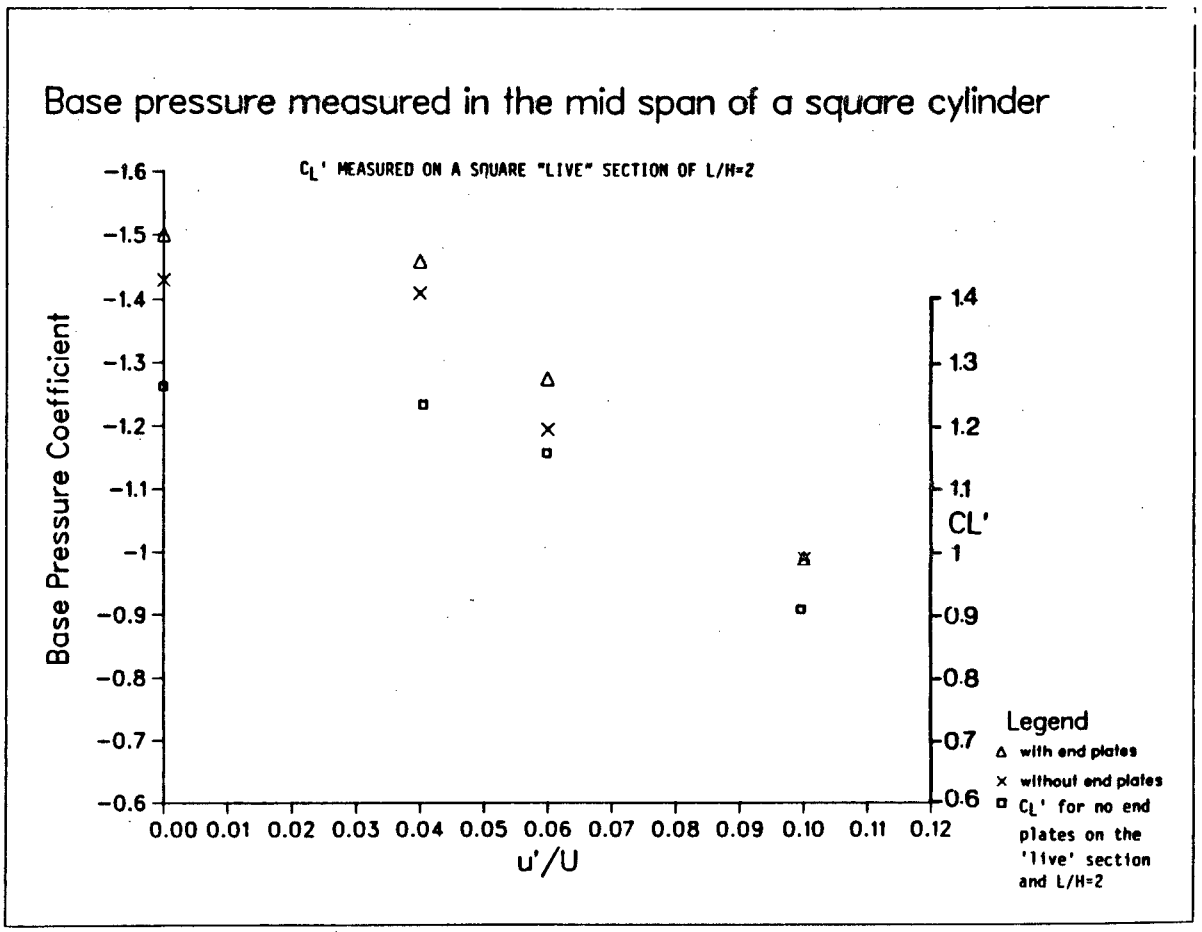

Figure 21: Variation of C_L' and C_{p_b} with turbulence intensity.

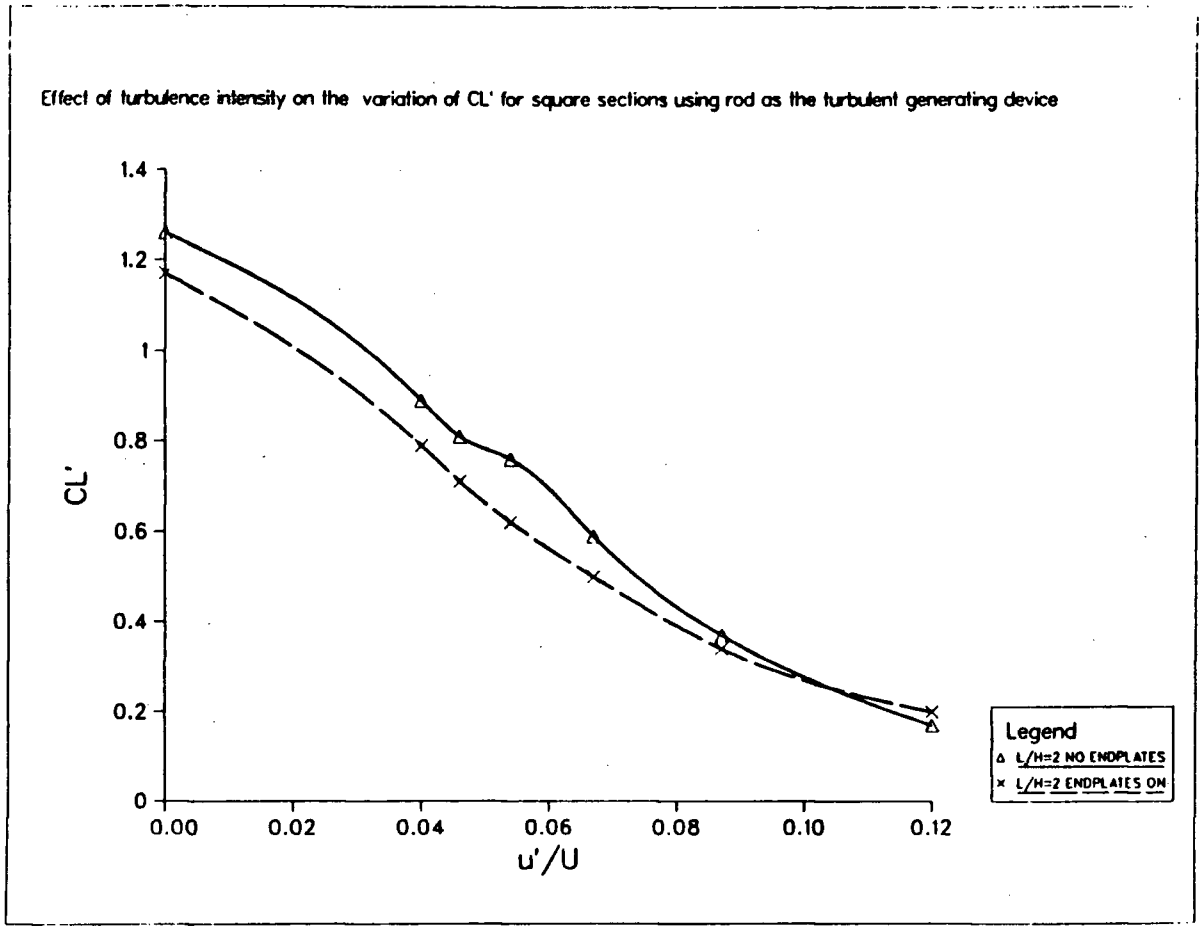

Figure 22: C_L' as a function of u'/U for a square section with L/H=2 (rod turbulence)

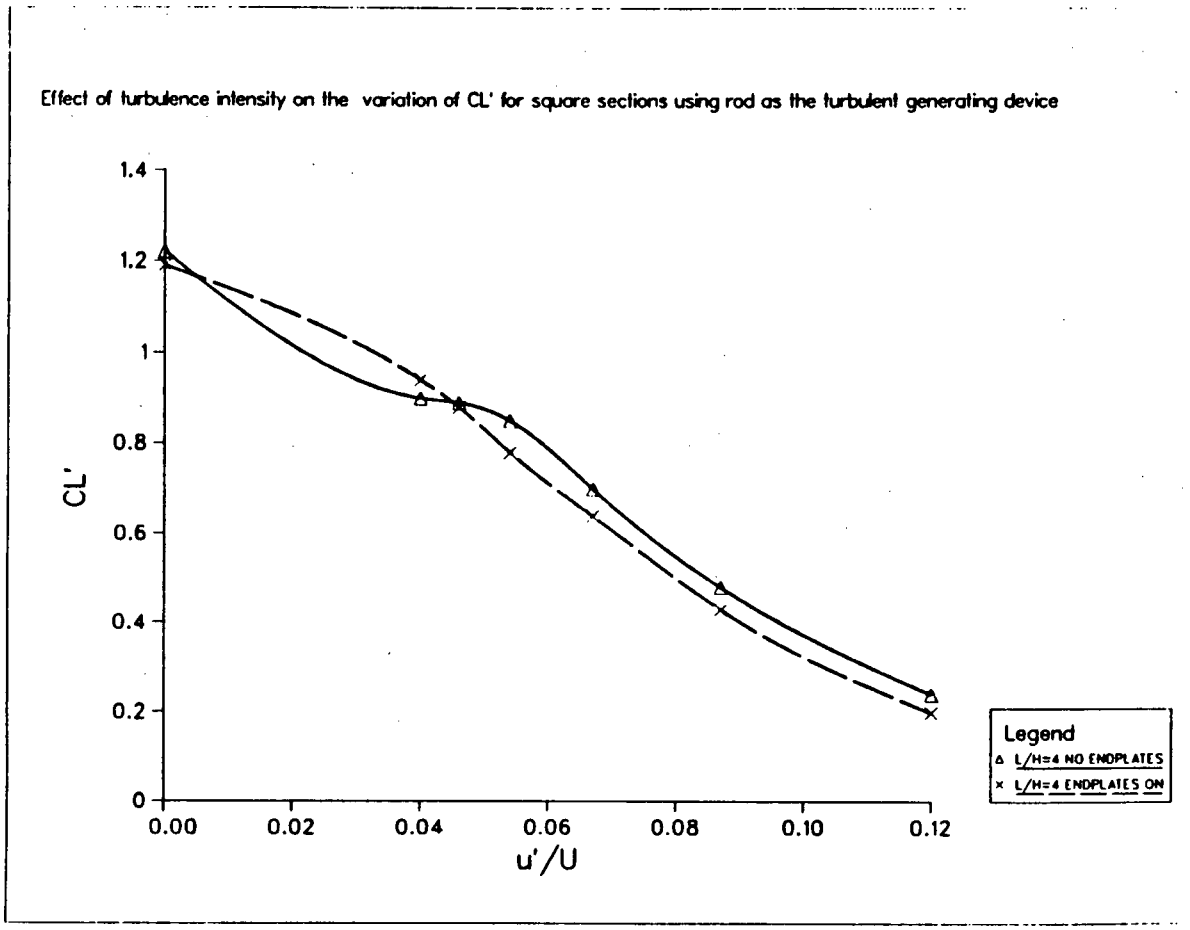

Figure 23: C_L' as a function of u'/U for a square section with L/H=4 (rod turbulence)

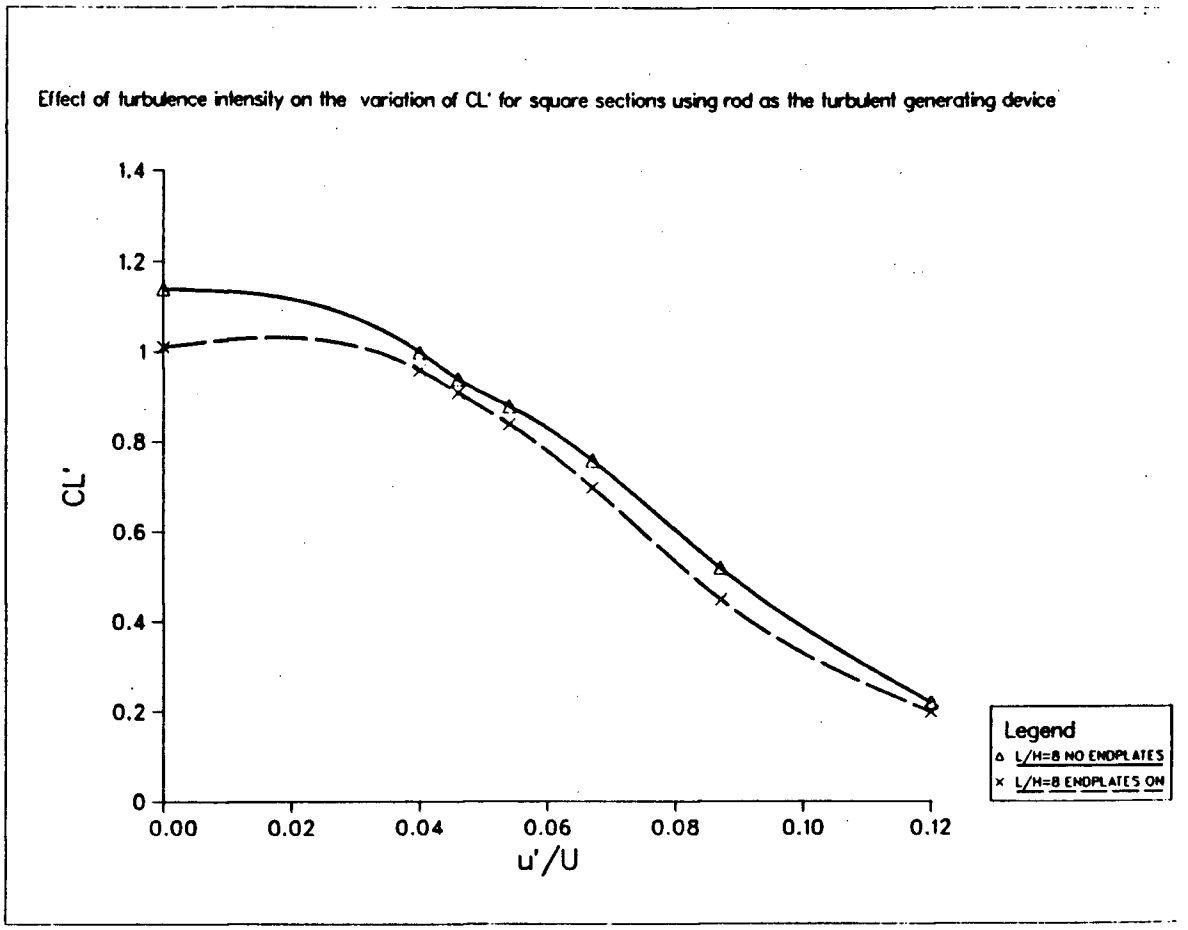

Figure 24: C_L' as a function of u'/U for a square section with L/H=8 (rod turbulence)

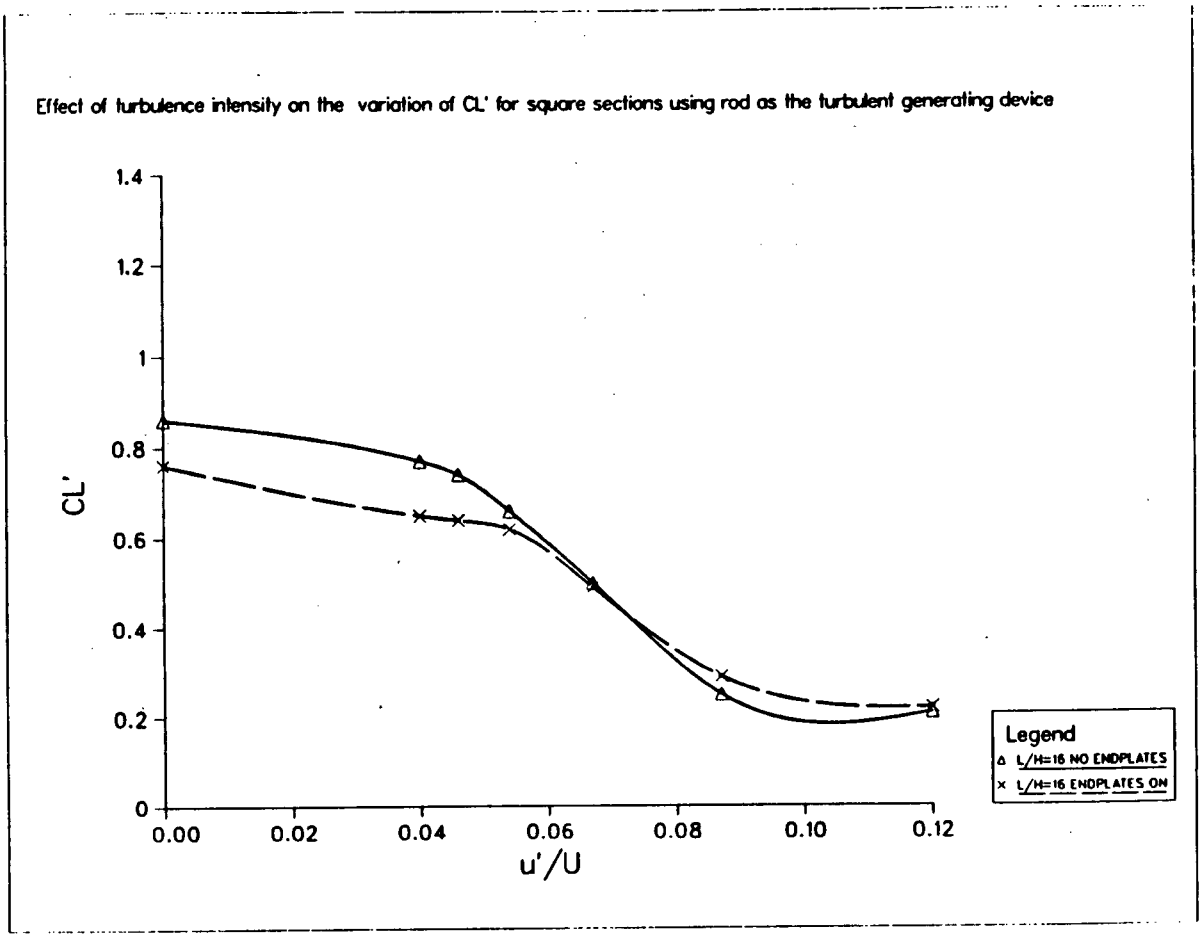

Figure 25: C_L' as a function of u'/U for a square section with L/H=16 (rod turbulence)

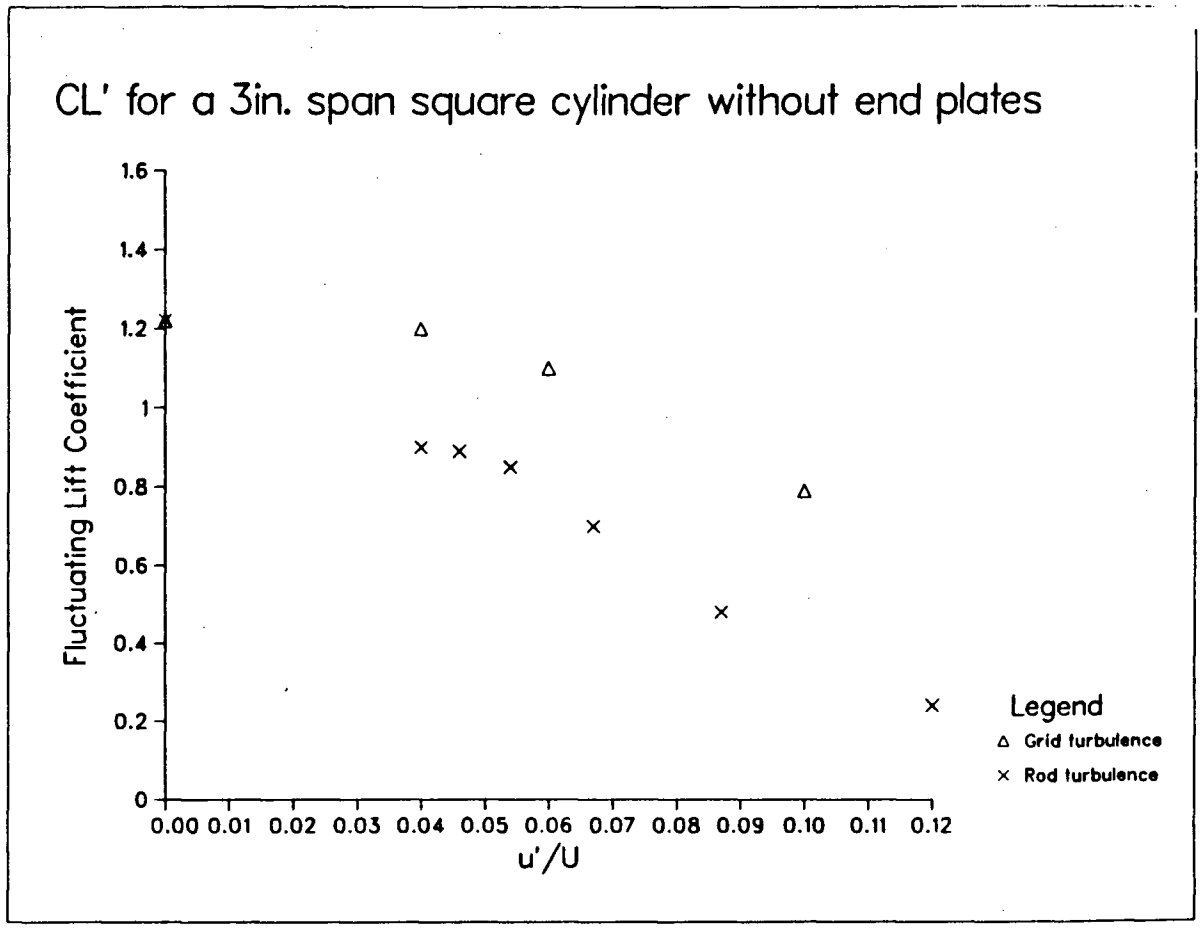

Figure 26: Comparison between C_L' obtained using rod and grid turbulence

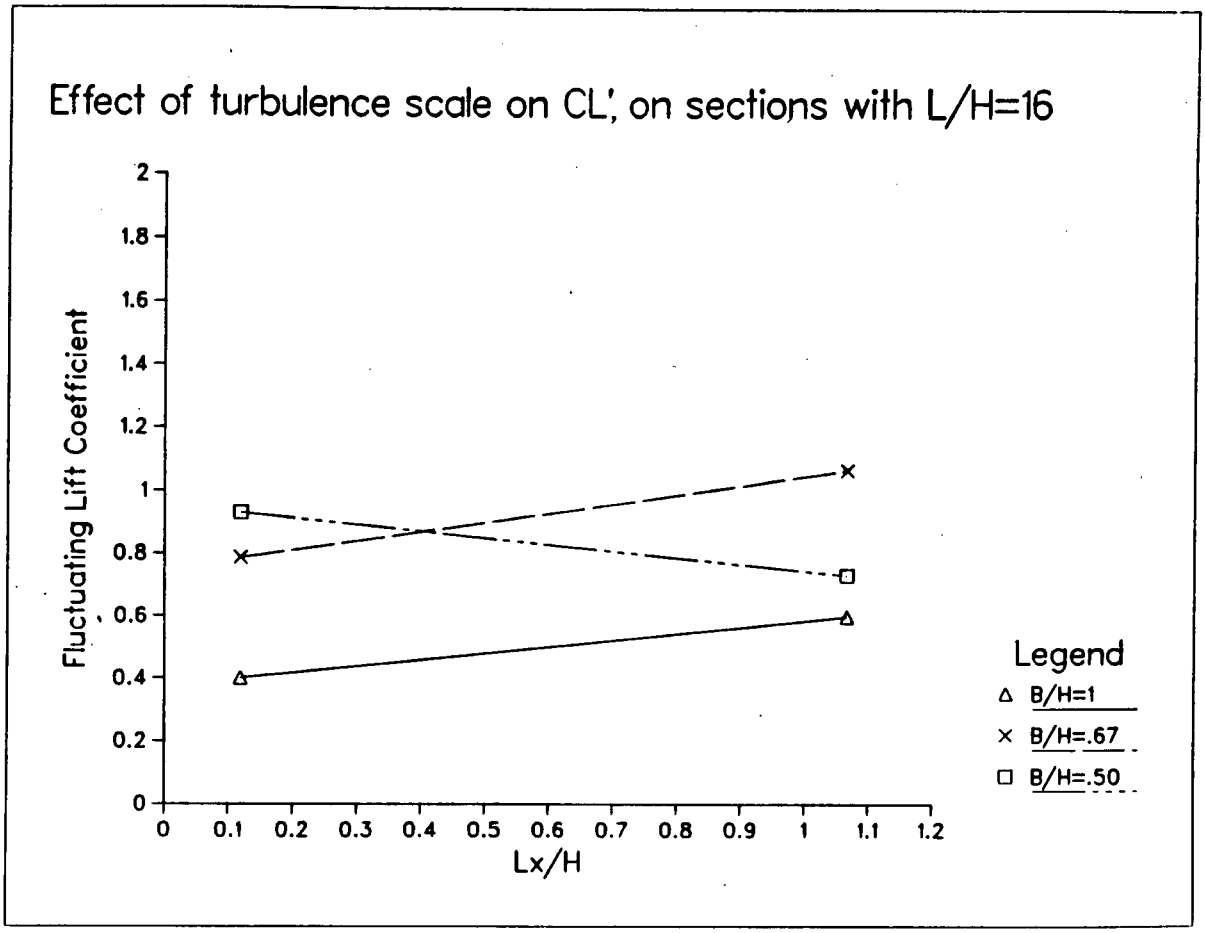

Figure 27: Effect of integral length scale on C_L'

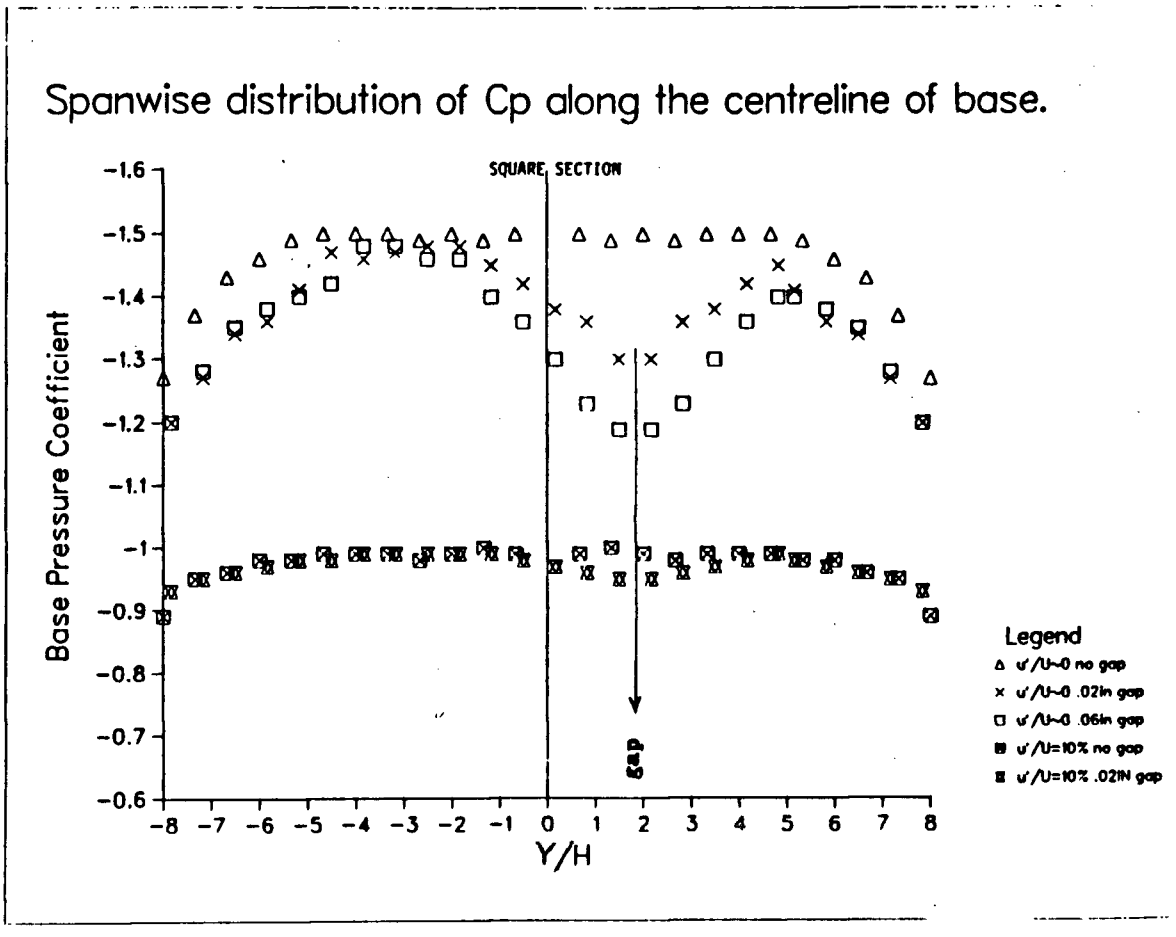

Figure 28: Effect of gap size (between the dummy end pieces and the 'live' section) on the mean base pressure coefficient.

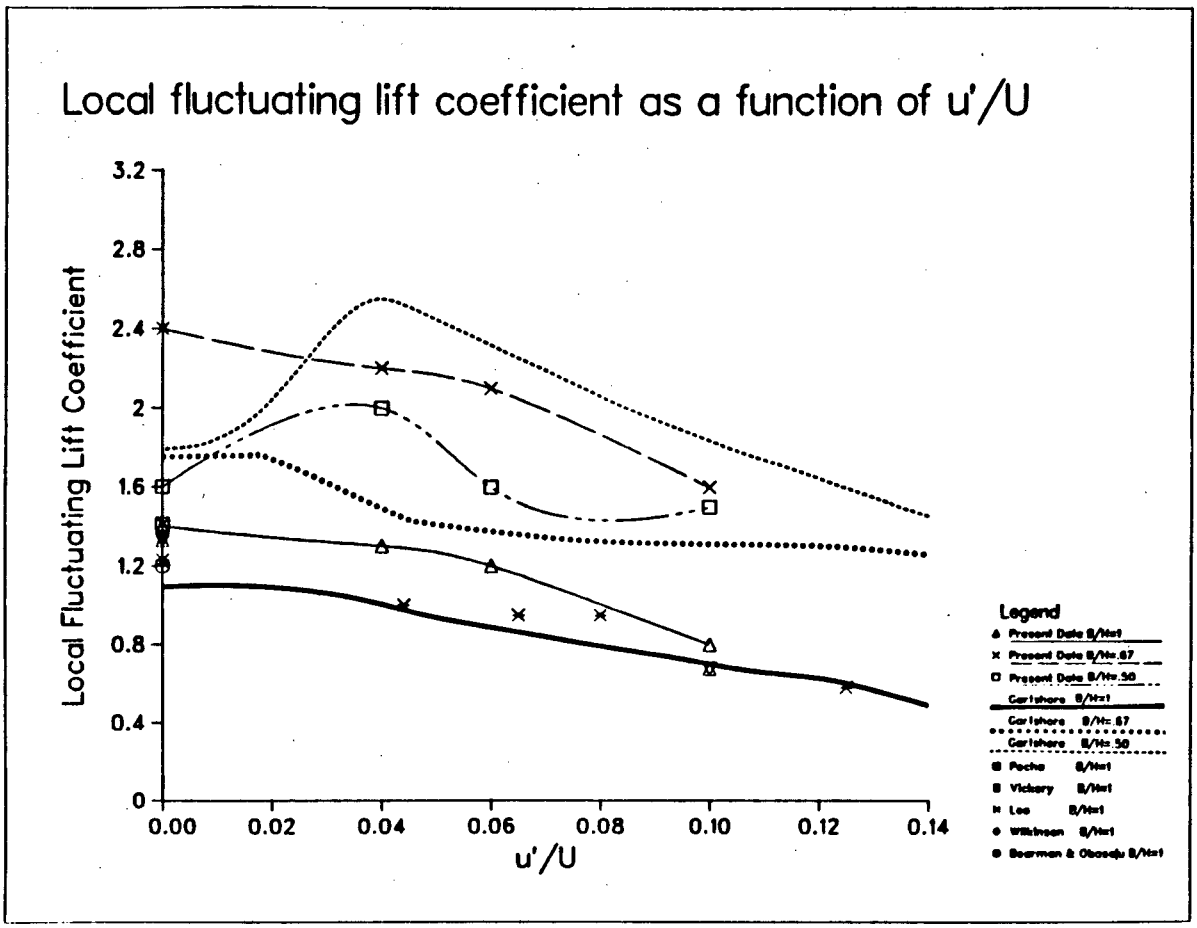

Figure 29: C'_{L_o} as a function of u'/U

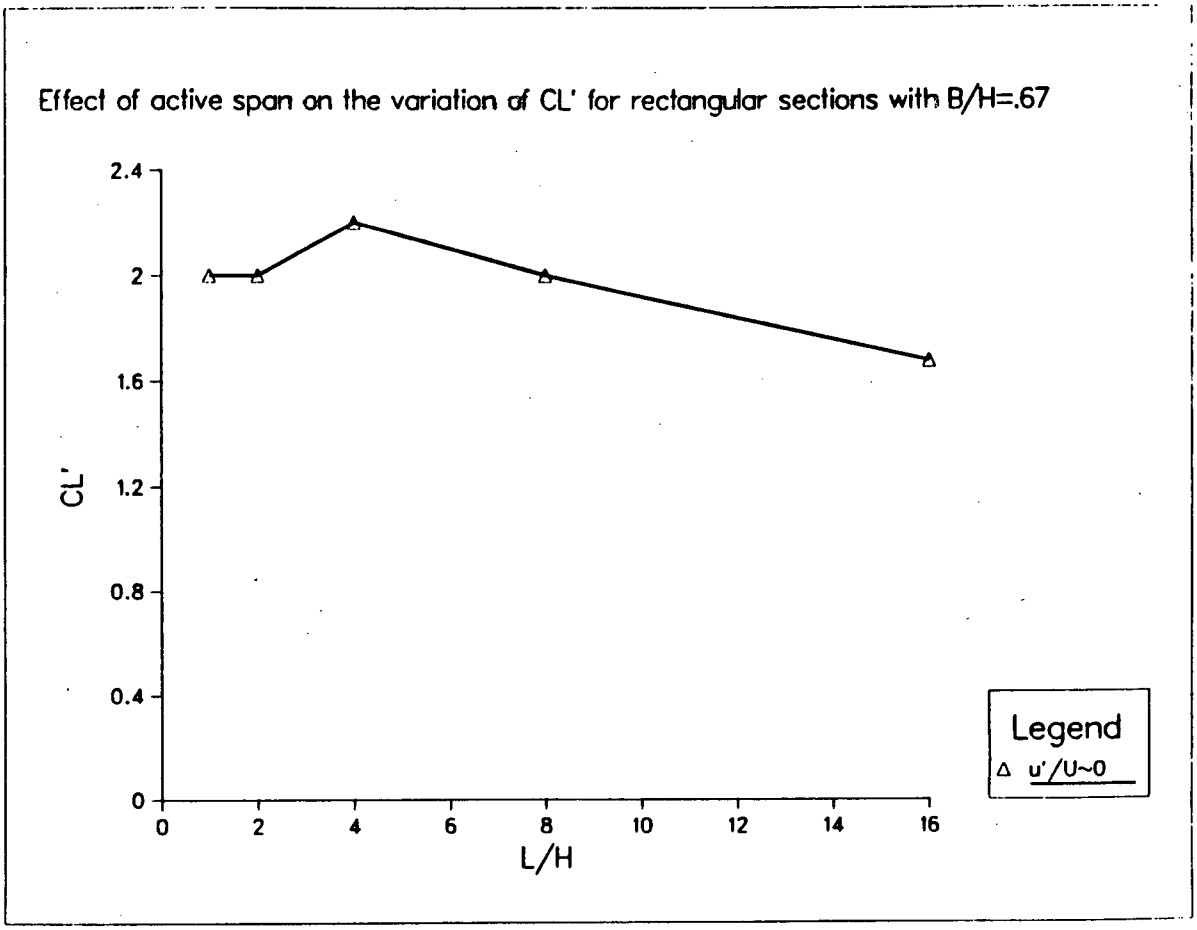

Figure 30: C_L' as a function of aspect ratio for cylinders with B/H=.67 at u'/U≃0

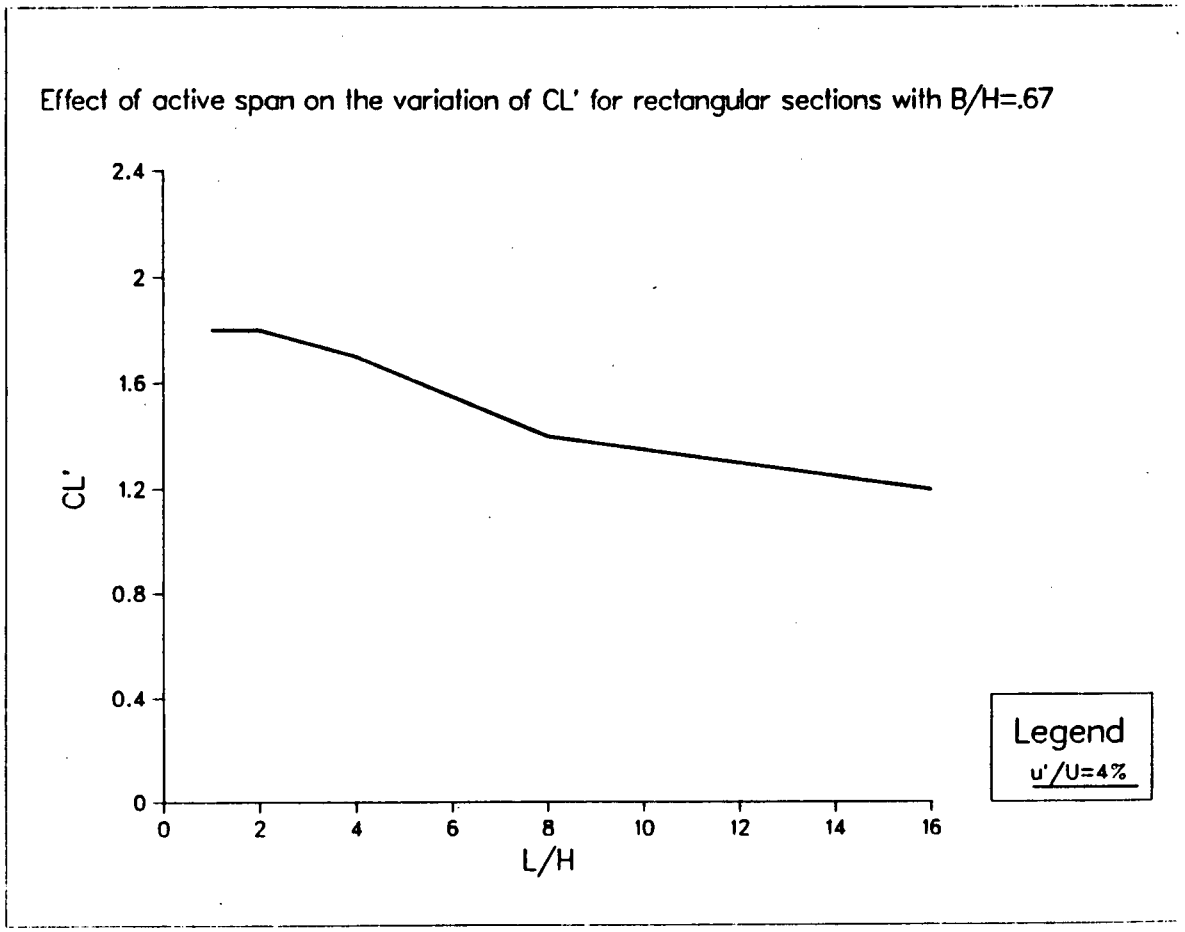

Figure 31: C_L' as a function of aspect ratio for cylinders with B/H=.67 at u'/U=4%

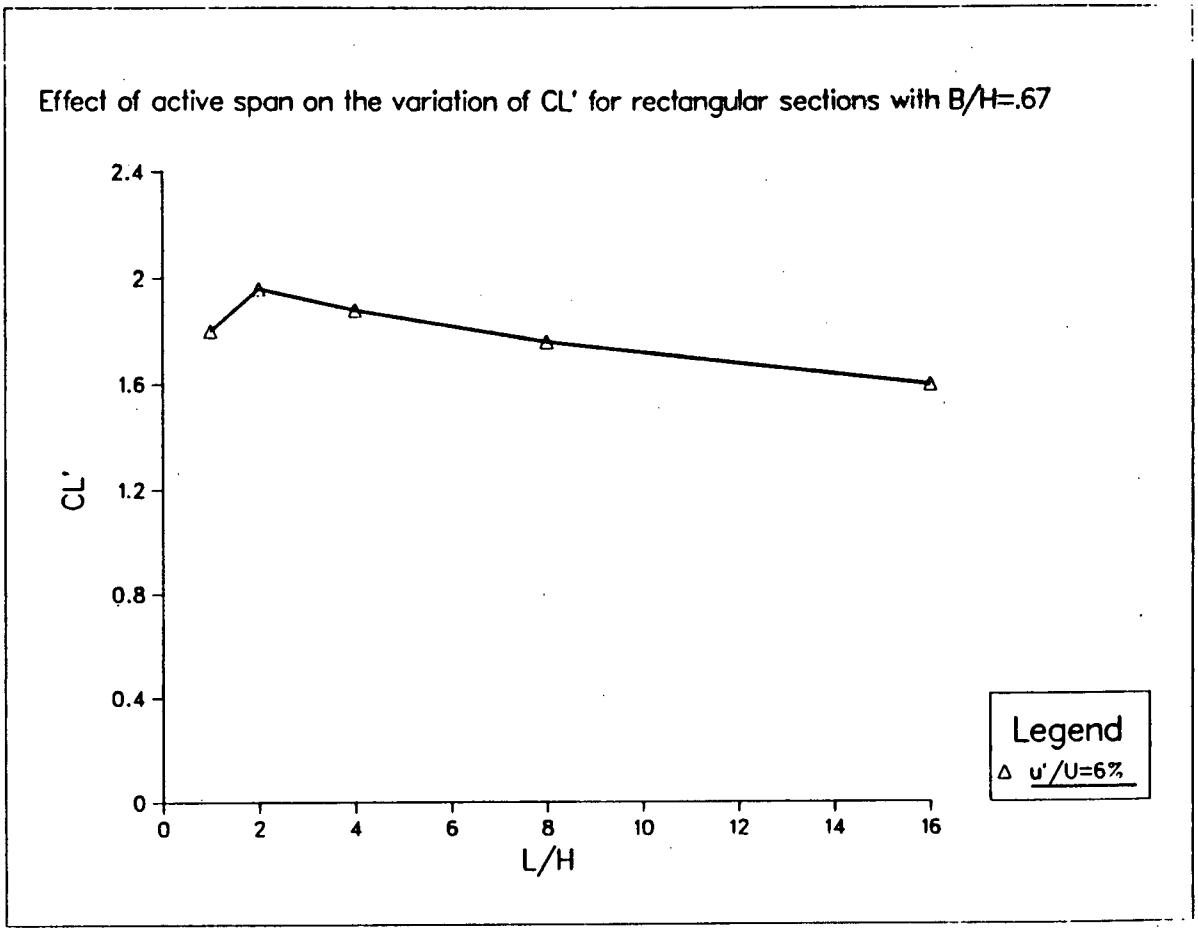

Figure 32: C_L' as a function of aspect ratio for cylinders with B/H=.67 at u'/U=6%

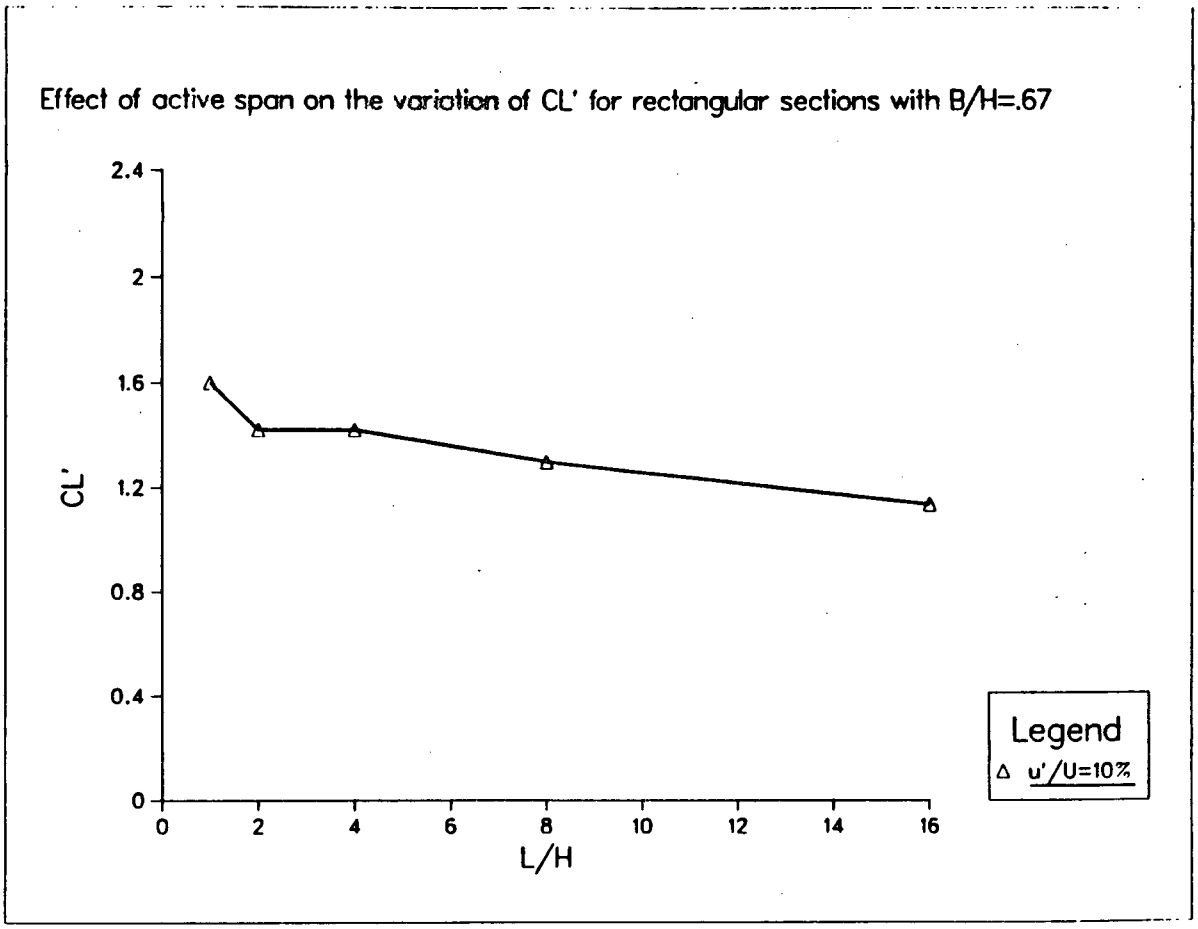

Figure 33: C_L' as a function of aspect ratio for cylinders with B/H=.67 at u'/U=10%

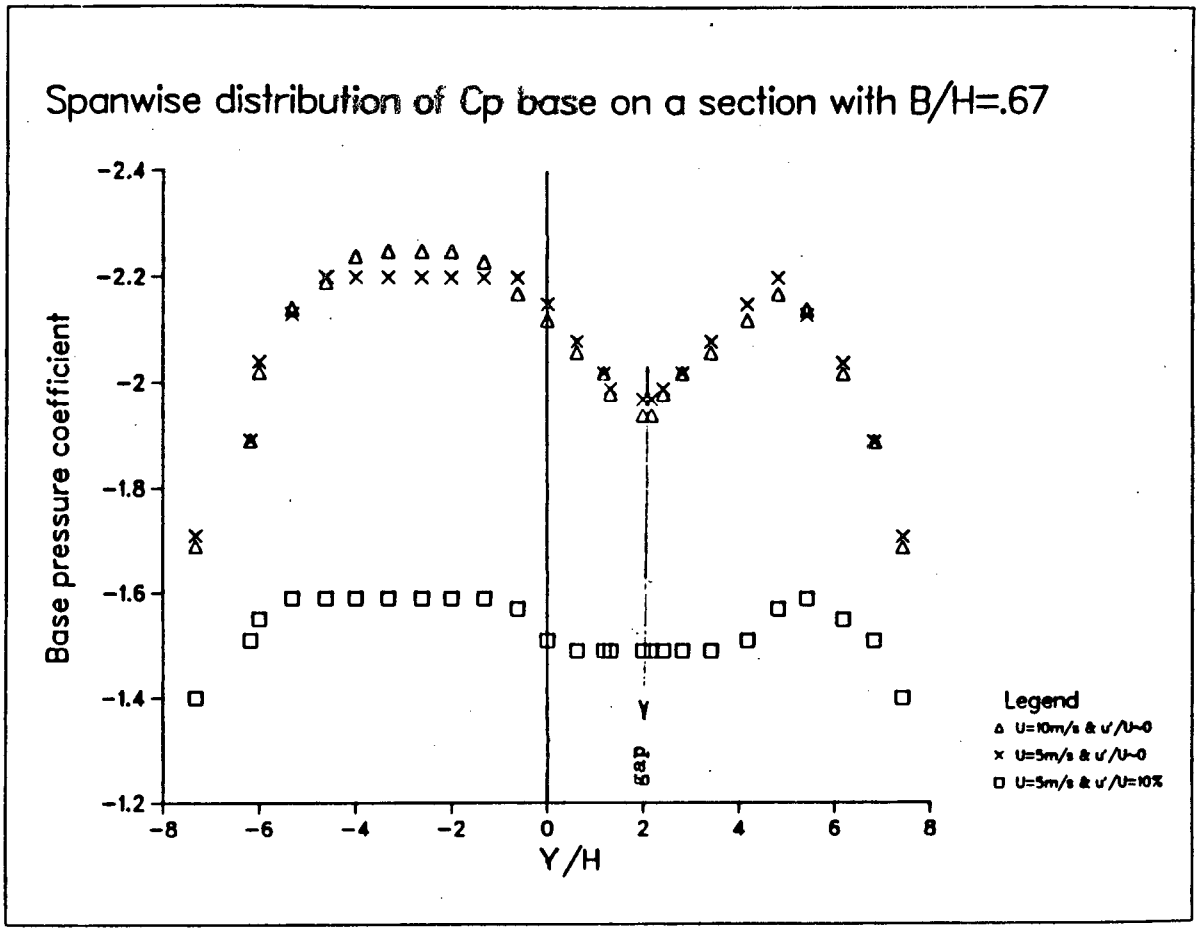

Figure 34: Base pressurre coefficient in smooth and turbulent flow for section with B/H=.67

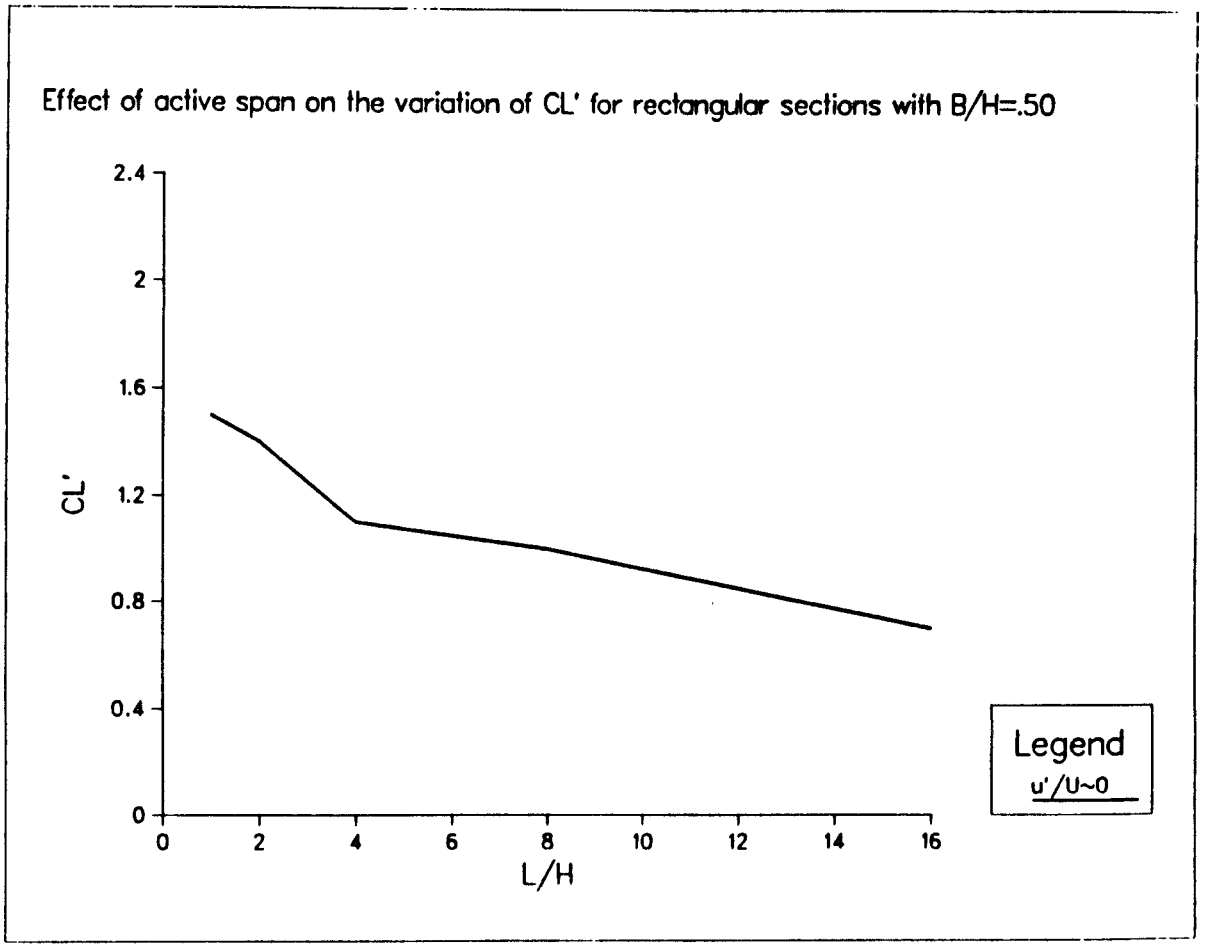

Figure 35: C_L' as a function of aspect ratio for cylinders with B/H=.50 at u'/U≃0

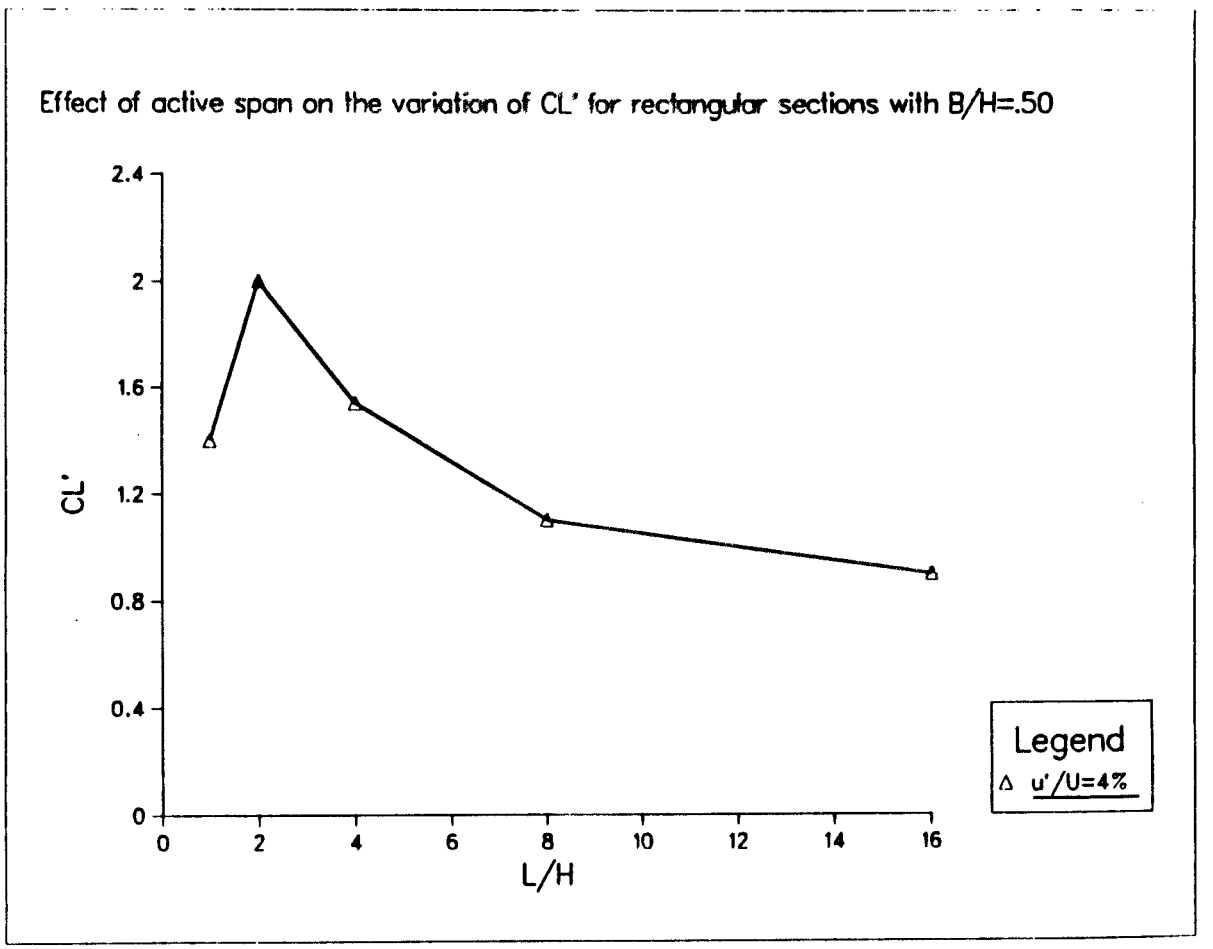

Figure 36: C_L' as a function of aspect ratio for cylinders with B/H=.50 at u'/U=4%

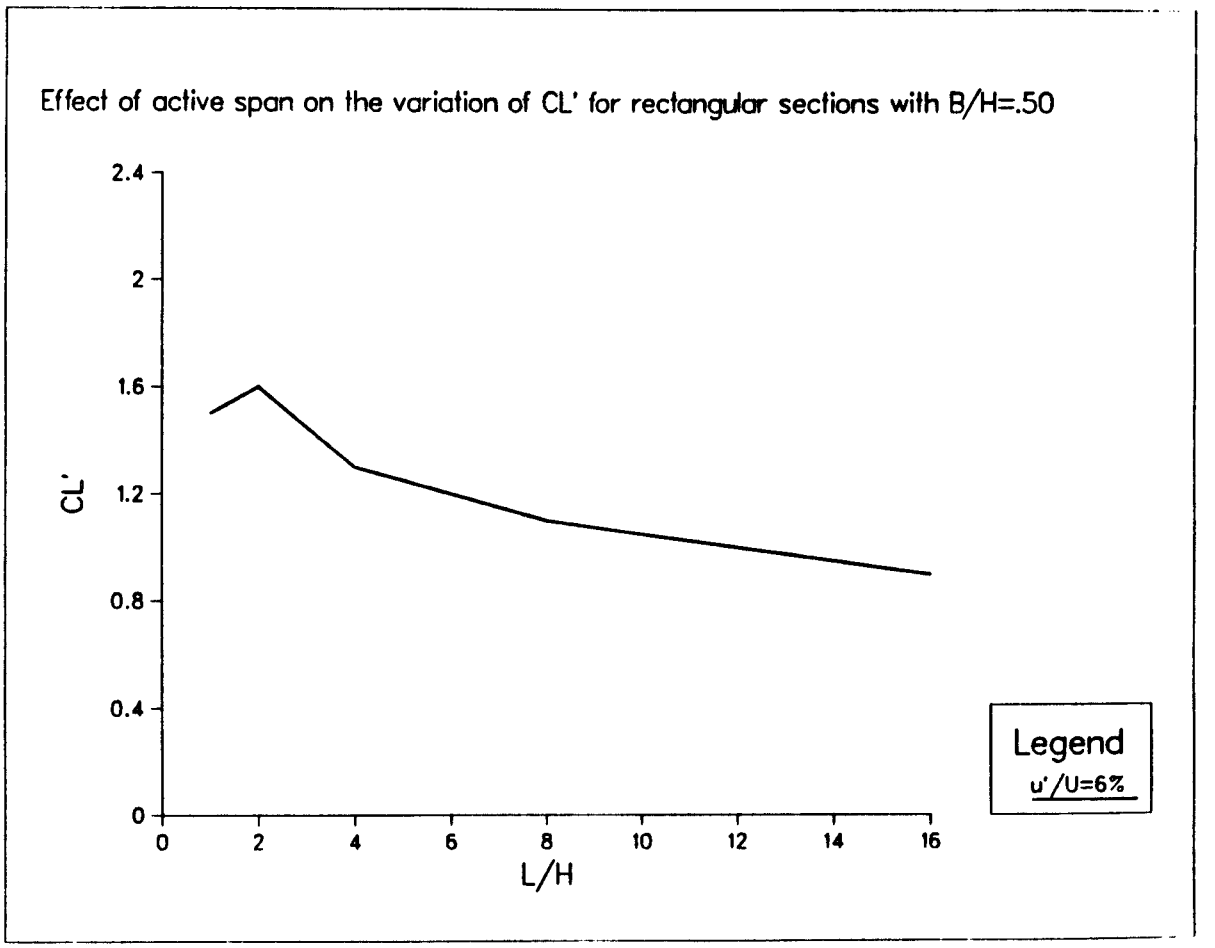

Figure 37: C_L' as a function of aspect ratio for cylinders with B/H=.50 at u'/U=6%

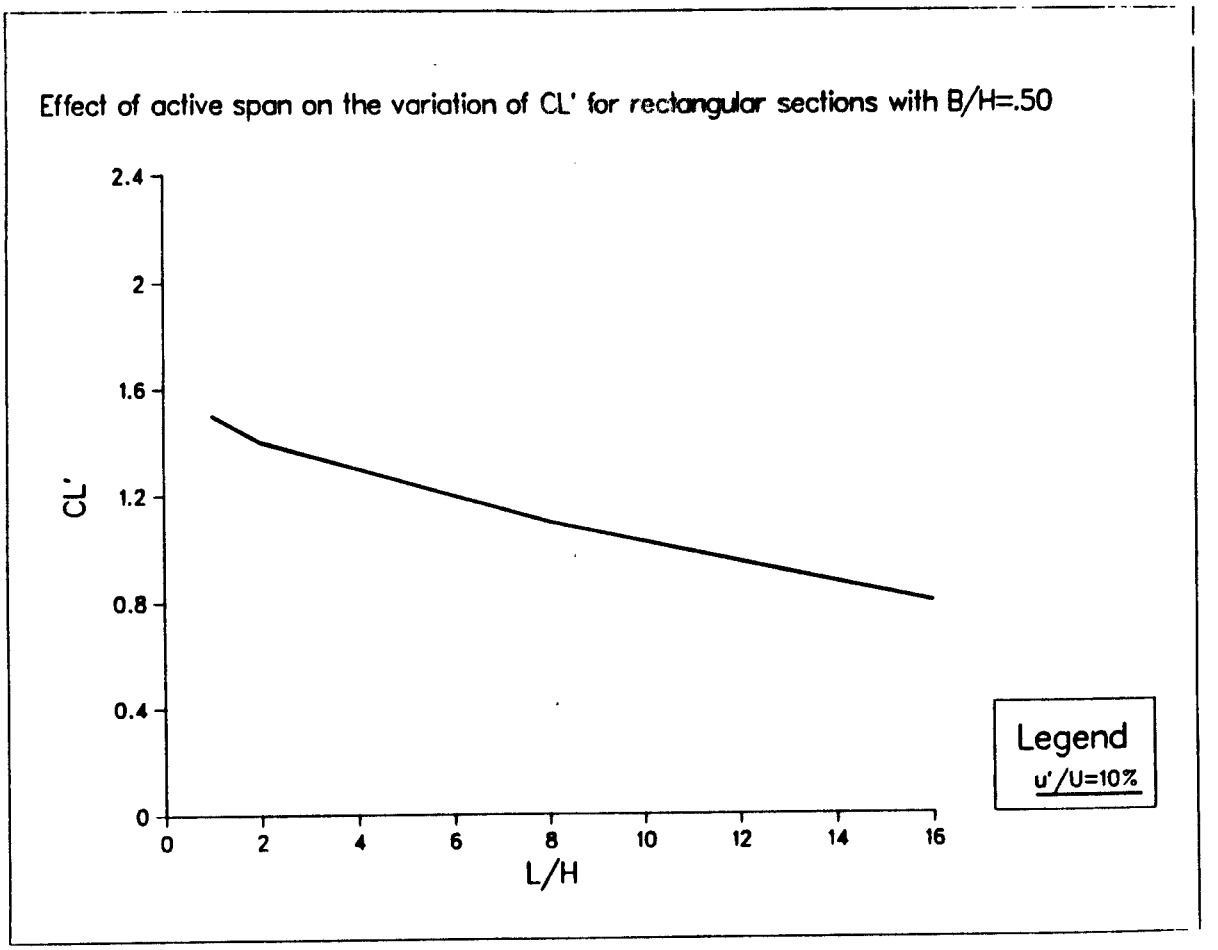

Figure 38: C_L' as a function of aspect ratio for cylinders with B/H=.50 at u'/U=10%

APPENDIX A

a) Hot Wire Calibration:

The calibration for the hot wire was found to be DC(volts)=K·U(m/s) where K=.49 for an air temperature of 82 degrees F, which was held approximately constant during the hot wire test. The following figure shows the calibration curve for the hot wire.

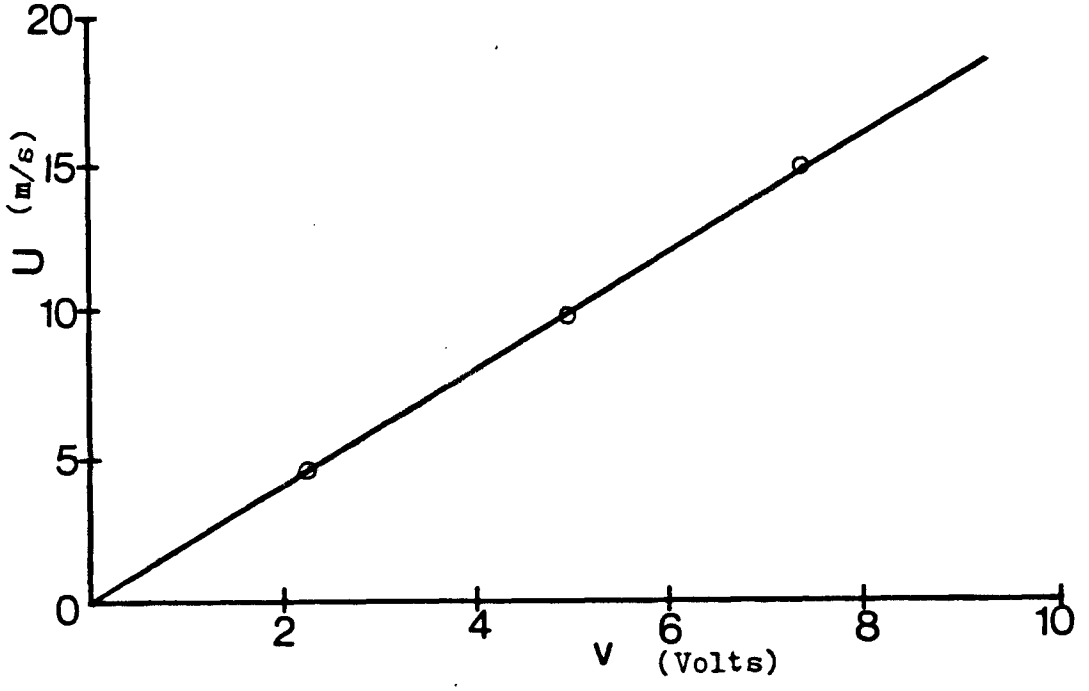

b)Length Scale:

A typical auto correlation curve is shown below. Integral time scale $T=\int_0^\infty R_U(\tau)d\tau$ was found, measuring the area under the curve. Using Taylor's hypothesis, integral length scale L_x was deduced: $L_x=U\cdot T$

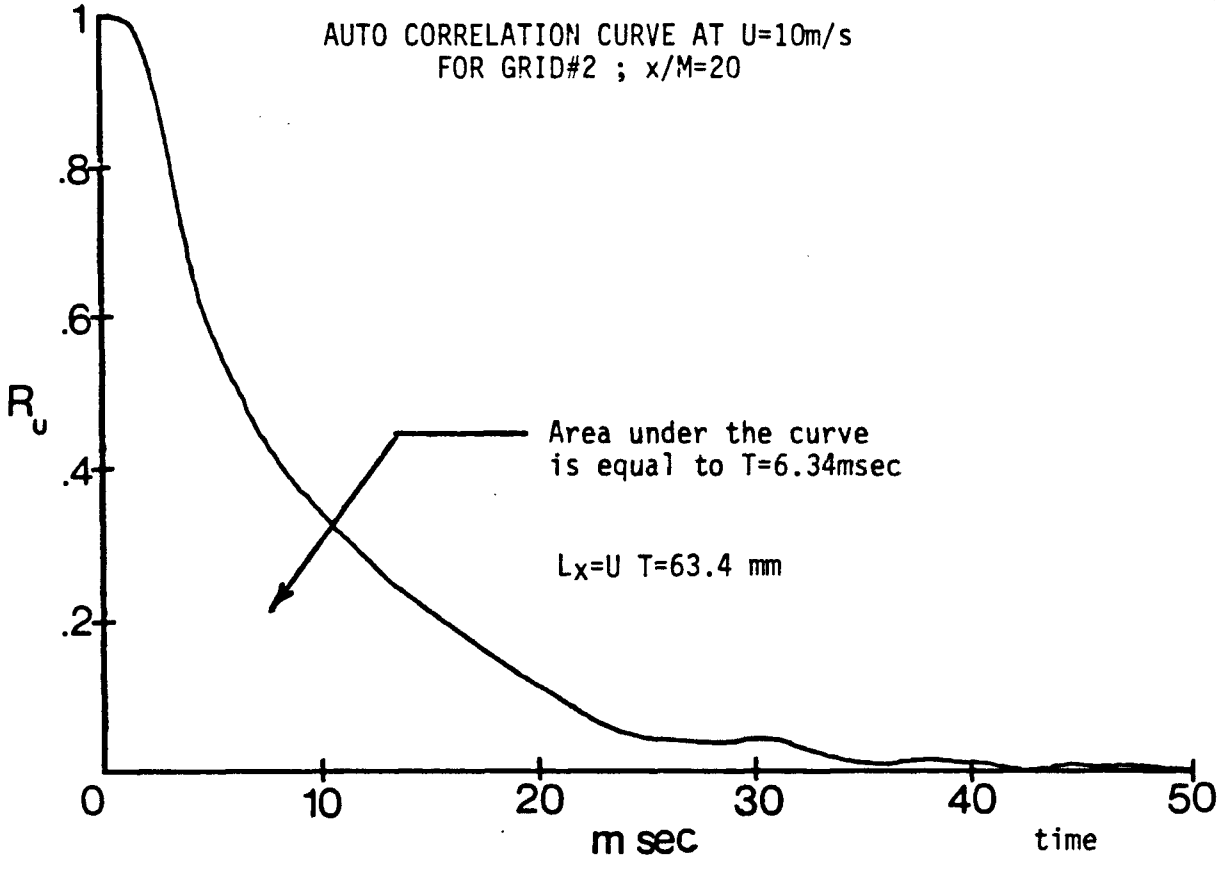

c)Filter calibration:

The filter calibration curve was obtained using a signal generator. The amplitude (i.e. voltage) of the generated sinusoidal signal was measured by a true-r.m.s. voltmeter. Then, this signal having a certain frequency, was fed into the amplifier, then into the filter with a certain low pass setting and finally into the same true-r.m.s. voltmeter. The following calibration curves are obtained by varying the signal frequency for certain filter low pass settings.

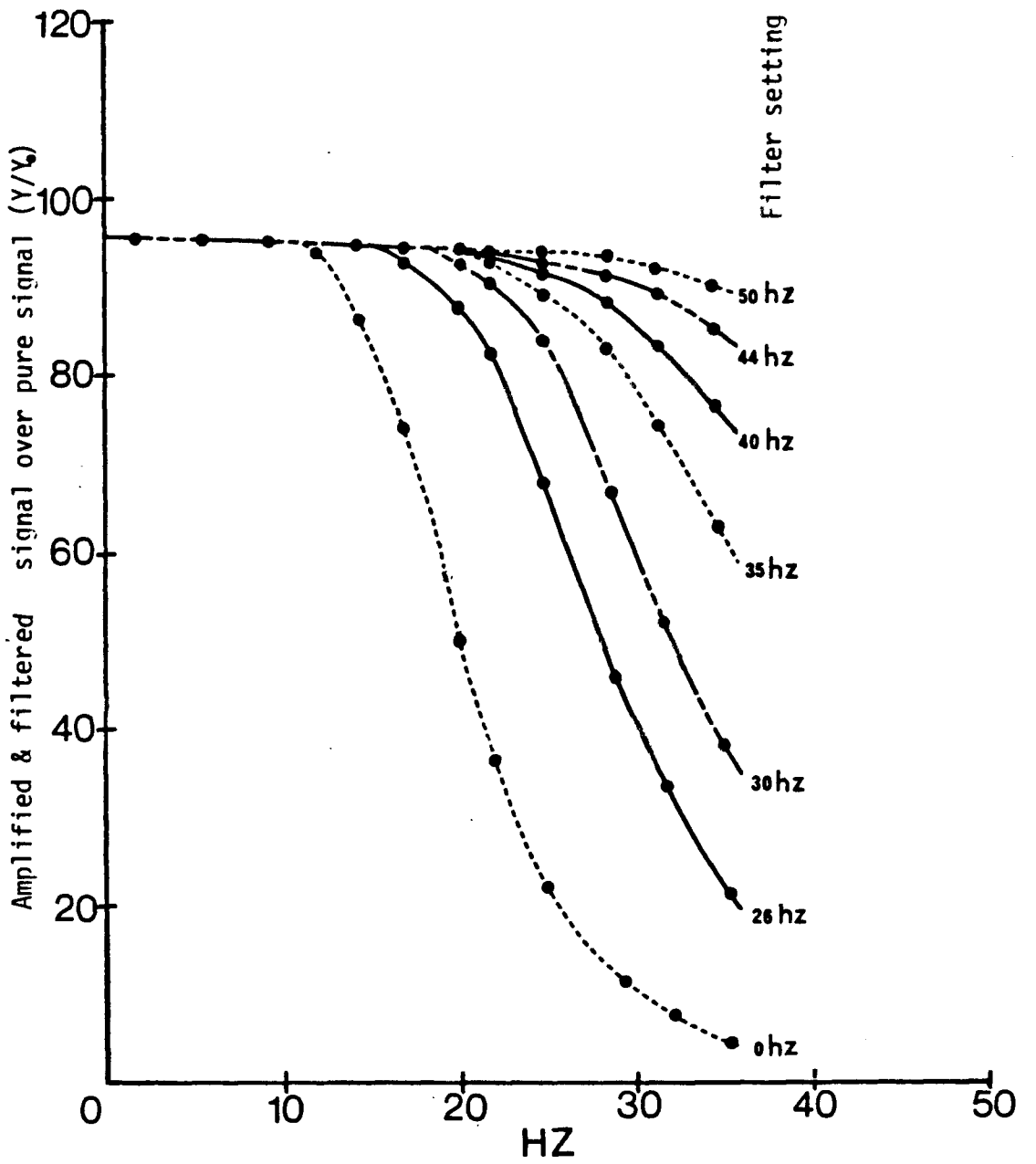

APPENDIX B

Methods of measuring r.m.s. fluctuating lift coefficient by using a simple beam as a load cell

Consider a beam clamped at both ends exposed to a concentrated load at its centre span varying sinuosoidally with time. The equation for one degree of freedom motion can be written as :

$$m\ddot{x}+c\dot{x}+kx=F(t)=F_1Sin(\omega_1 t)+F_2Sin(\omega_2 t)+...$$

For one sinusoidal load, the equation of motion is:

$$m\ddot{x}+c\dot{x}=F(t)=F_1Sin(\omega_1 t)$$

$$\ddot{x}+(c/m)\dot{x}+(k/m)x=(F_1/m)Sin\omega_1 t$$

Defining $\beta=c/(4mk)^{1/2}$ as the fraction of critical damping and $\omega_n=(k/m)^{1/2}$ as the natural frequency, then the equation can be written as:

$$\ddot{x}+2\beta\omega_n\dot{x}+\omega_n^2x=(F_1/m)Sin\omega_1 t$$

The solution to the above equation is:

$$x(t)=(F_1/k)H(\omega_1)Cos(\omega_1 t-\phi_1)$$

where $H(\omega)$ is the mechanical admittance and is:

$$H(\omega)=\{[1-(\omega/\omega_n)^2]^2+(2\beta\omega/\omega_n)^2\}^{-1/2}$$

and ϕ is the phase angle and is:

$$\phi=\tan^{-1}\{2\beta(\omega/\omega_n)/[1-(\omega/\omega_n)^2]\}$$

The square of the solution function is:

$$x^2(t)=[(F_1/k)H(\omega_1)Cos(\omega_1 t-\phi_1)]^2$$

Time averaging:

$$\overline{x^2}= (\overline{F^2}/k^2)H^2(\omega)$$

where $\overline{F^2}=\overline{F_1^2 Sin^2(\omega t)}=F_1^2/2$

For a variety of loading frequencies, this result may be expressed in the form of spectra, defined as:

$$\overline{x^2}=\int_0^\infty S_{XX}(\omega)d\omega \text{ and } \overline{F^2} =\int_0^\infty S_{FF}(\omega)d\omega$$

In both cases the spectra represents the contribution to $\overline{x^2}$ or $\overline{F^2}$ from frequencies near ω. Hence

$$S_{XX}(\omega)=(1/k^2)H^2(\omega)S_{FF}(\omega)$$

and $$\overline{x^2}=\int_0^\infty (1/k^2)H^2(\omega)S_{FF}(\omega)d(\omega)$$

If $S_{FF}(\omega)$ is narrow and is in a range not close to ω_n then $H(\omega)$ over this range may be considered approximately constant and equal to $H(\omega_v)$ where $S_{FF}(\omega_v)$ is the peak of the force spectrum (i.e. the frequency ω_v is the vortex shedding frequency). With this assumption:

$$\sqrt{\overline{x^2}}=(1/k)H(\omega_v)\ \sqrt{\overline{F^2}}$$

Writing $\sqrt{\overline{F^2}}$ in terms of an r.m.s. lift coefficient C_L', where $\sqrt{\overline{F^2}} = 1/2\rho U^2 L B C_L'$ then:

$$C_L' = \frac{\sqrt{\overline{x^2}}/B}{H(\omega_V)} \quad \frac{k}{1/2\rho U^2 L}$$

This equation was used to calculate C_L' from measured values of $\sqrt{\overline{x^2}}$, f_V, U, L and B with k known from calibration.

APPENDIX C

Effect of aspect ratio on the fluctuating lift coefficients.

a)- Model with no end effects:

By definition:

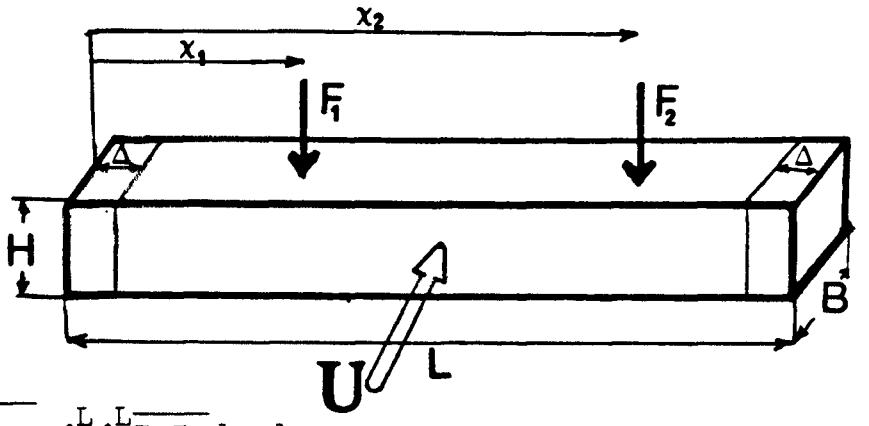

$$\overline{F_B^2}=\overline{\int_0^L F_1 dx_1 \int_0^L F_2 dx_2}=\int_0^L\int_0^L \overline{F_1 F_2}\, dx_2 dx_1$$

where $\overline{F_B^2}$ is the mean square force on the entire body where as F_1 and F_2 are local forces per unit length.

Defining the force correlation coefficient as:

$$R_{FF}=\frac{\overline{F_1 F_2}}{\overline{F_0^2}} \qquad \text{where } \overline{F_0^2}=\overline{F_1^2}=\overline{F_2^2}$$

then

$$\overline{F_B^2}=\overline{F_0^2}\int_0^L\int_0^L R_{FF}\, d(x_1-x_2)dx_1 dx_2$$

Considering a simple form for R_{FF} as $R_{FF}=\exp(-A|x_1-x_2|)$ and substituting in equation for $\overline{F_B^2}$ and integrating, while knowing that $\int^{\infty} R_{FF}\, d(x_1-x_2)=\lambda$ and $\sqrt{\overline{F_B^2}}=C_L' \; 1/2\rho U^2 LB$ and $\overline{F_0^2}=C_{L_0}' \; 1/2\rho U^2 B$ we get:

$$C_L'=C_{L_0}'\sqrt{2}\lambda/L[L/\lambda -1+\exp(-L/\lambda)]^{1/2}$$

In this expression,

$C_L' \rightarrow C_{L_0}'$ if $L/\lambda \ll 1$

and $C_L' \rightarrow C_{L_0}'(2\lambda/L)^{1/2}$ if $L/\lambda \gg 1$

b)- Model with end effects:

Assume Δ is the length representing the loss of lift due to each end. Then:

$$\overline{F_B^2} = \overline{F_0^2} \int_{\Delta}^{L-\Delta} \int_{\Delta}^{L-\Delta} R_{FF}(x_1-x_2)dx_1dx_2$$

Making the same assumptions as in part (a) and carrying out the integrations we find:

$$C_L' = C_{L_0}' \sqrt{2}\lambda/L[L'/\lambda - 1 + \exp(-L'/\lambda)]^{1/2} \qquad \text{where } L' = L-2\Delta$$